UCID--21362-Vol.6

DE90 006352

Survey of Degradation Modes of Candidate Materials for High-Level Radioactive-Waste Disposal Containers

Volume 6
Effects of Hydrogen in Austenitic and Copper-Based Alloys

G. E. Gdowski and D. B. Bullen
Science & Engineering Associates, Inc.
Pleasanton, Calif.

August 1988

LAWRENCE LIVERMORE NATIONAL LABORATORY
University of California • Livermore, California • 94550

Contents

List of Volumes of the Survey

This is Volume 6 of the report *Survey of Degradation Modes of Candidate Materials for High-Level Radioactive-Waste Disposal Containers*. The titles of all of the volumes are as follows:

Overview
Volume 1: Phase Stability
Volume 2: Oxidation and Corrosion
Volume 3: Localized Corrosion and Stress Corrosion Cracking of Austenitic Alloys
Volume 4: Stress Corrosion Cracking of Copper-Based Alloys
Volume 5: Localized Corrosion of Copper-Based Alloys
Volume 6: Effects of Hydrogen in Austenitic and Copper-Based Alloys
Volume 7: Weldability of Austenitic Alloys
Volume 8: Weldability of Copper-Based Alloys

Acronyms

BWR	boiling-water reactor
CDA	Copper Development Association
CHLW	commercial high-level waste
DHLW	defense high-level waste
HAZ	heat-affected zone
NNWSI	Nevada Nuclear Waste Storage Investigations Project
ppm	parts per million
PWR	pressurized-water reactor
SCG	slow crack growth
SEM	scanning electron microscopy
TEM	transmission electron microscopy
UTS	ultimate tensile strength
YS	yield stress

Executive Summary

This volume discusses the effects of hydrogen on the six candidate materials for the metal containers to be used in disposing of high-level radioactive waste. Three of the candidate materials are iron- to nickel-based austenitic materials: Types 304L and 316L stainless steels and Alloy 825. The other three are copper-based alloys: CDA 102 (oxygen-free copper), CDA 613 (Cu-7Al), and CDA 715 (Cu-30Ni). These materials, particularly the copper alloys, are used extensively in marine environments. The austenites are used extensively in the nuclear industry.

Radioactive waste will be sent to the prospective repository at Yucca Mountain, Nevada, for disposal. Disposal containers can undergo several forms of degradation during their lifetimes in the repository. The selection of the candidate material that is adequate for repository conditions will be based on three tasks: a literature survey, corrosion testing, and predictions from modeling. Lawrence Livermore National Laboratory has responsibility for all three. This volume surveys the literature on the effect of hydrogen on the candidate materials. Other volumes address phase stability, general oxidation and corrosion, localized corrosion, and stress corrosion cracking.

Section 1 is an introduction to the high-level radioactive-waste project at Yucca Mountain. The gamma radiation field from the decay of the high-level waste may promote radiolytic decomposition of water to hydrogen.

Sections 2 through 5 discuss the effect of hydrogen on the copper-based alloys. In copper, the deleterious effect caused by hydrogen is the formation of cavities on grain boundaries. These cavities are formed by the reduction of cuprous oxide (Cu_2O) at grain boundaries. The voids are stabilized by the water vapor molecules and grow as more cuprous oxide is reduced along the same grain boundary. Cuprous oxides can be formed in copper during casting and welding. These oxides are not wetted by molten copper and are therefore swept to grain boundaries during solidification. Brittle failure and losses in plasticity of over 50% have been reported. This effect occurs at an oxygen concentration as low as 22 atomic ppm. These problems may be alleviated by the use of a deoxidizer.

The solubility, diffusivity, and permeability of hydrogen in copper are reviewed in Sec. 3. These properties are usually obtained at high temperatures because of their extremely low values near room temperature. Therefore, extrapolation to repository-relevant temperatures is usually required. Hydrogen is most soluble in copper-nickel alloys.

Tests have shown that the hydrogen charging of copper and copper-aluminum alloys without internal oxides reduces the fracture strain by about 5%. No data were found for copper-nickel alloys. In terms of resistance to the detrimental effects of hydrogen, the following ranking is proposed for the copper-based alloys: CDA 715 (best) > CDA 613 > CDA 102 (worst).

Sections 6 through 10 discuss the effects of hydrogen on the austenitic materials. Because of the limited solubility of hydrogen under normal conditions, severe cathodic charging conditions have often been employed. Hydrogen primarily degrades these materials by causing a loss in ductility, i.e., the failure becomes brittle. Losses in ultimate tensile strength and 0.2% yield strength are noted but are not as large as the losses in ductility. Recovery of the mechanical properties has been observed after aging in hydrogen-free atmospheres. The mechanism of hydrogen embrittlement of the austenitics is not known.

There is significant documentation to show that Type 316L stainless steel is less susceptible than Type 304L stainless steel to hydrogen embrittlement at room temperature. Sensitized alloys and coarse-grained alloys are more susceptible to hydrogen embrittlement, although the susceptibility of fine-grained Type 316L stainless steel is the same whether it is sensitized or not. Little documentation exists for hydrogen embrittlement of Alloy 825, but what does exist suggests that it is about as susceptible as Type 316L stainless steel.

Some studies have indicated that Type 304 stainless steel is less susceptible to cracking at elevated temperatures. Slow crack growth in hydrogen gas was reported at 25°C but not at 160°C. In addition, losses in ductility after hydrogen charging were 50% at 0°C but negligible at 107°C.

Section 8 documents the diffusivities and solubilities of hydrogen in Type 304 stainless steel and nickel. The properties of hydrogen are generally the same in similar austenitic stainless steels. Since no

studies have been performed on Alloy 825, data for hydrogen in nickel are presented to show the effect of larger nickel concentrations.

In terms of resistance to the detrimental effects of hydrogen, the following ranking is proposed for the austenitic alloys: Type 316L stainless steel ≈ Alloy 825 > Type 304L stainless steel.

Survey of Degradation Modes of Candidate Materials for High-Level Radioactive-Waste Disposal Containers

Volume 6: Effects of Hydrogen in Austenitic and Copper-Based Alloys

Abstract

Six alloys are being considered as possible materials for the fabrication of containers for the disposal of high-level radioactive waste. Three of these candidate materials are copper-based alloys: CDA 102 (oxygen-free copper), CDA 613 (Cu-7Al), and CDA 715 (Cu-30Ni). The other three are iron- to nickel-based austenitic materials: Types 304L and 316L stainless steels and Alloy 825. Radioactive waste will include spent-fuel assemblies from reactors as well as waste in borosilicate glass and will be sent to the prospective site at Yucca Mountain, Nevada, for disposal. The waste-package containers must maintain substantially complete containment for at least 300 yr and perhaps as long as 1000 yr. During the first 50 yr after emplacement, the containers must be retrievable from the disposal site. Shortly after emplacement of the containers in the repository, they will be exposed to high temperatures and high gamma radiation fields from the decay of high-level waste. This radiation will promote the radiolytic decomposition of moist air to hydrogen.

This volume surveys the available data on the effects of hydrogen on the six candidate alloys for fabrication of the containers. For copper, the mechanism of hydrogen embrittlement is discussed, and the effects of hydrogen on the mechanical properties of the copper-based alloys are reviewed. The solubilities and diffusivities of hydrogen are documented for these alloys. For the austenitic materials, the degradation of mechanical properties by hydrogen is documented. Some instances of property recovery are noted. The diffusivity and solubility of hydrogen in these alloys are also presented.

For the copper-based alloys, the ranking according to resistance to detrimental effects of hydrogen is: CDA 715 (best) > CDA 613 > CDA 102 (worst). For the austenitic alloys, the ranking is: Type 316L stainless steel ≈ Alloy 825 > Type 304L stainless steel (worst).

1. Introduction

The Nuclear Waste Management Program (NWMP) at Lawrence Livermore National Laboratory is responsible for the development of the waste-package design to meet the Nuclear Regulatory Commission licensing requirements for the containment of high-level waste. Waste will include: (1) spent fuel from civilian nuclear power plants, namely, fuel assemblies and consolidated fuel pins from pressurized-water reactors (PWRs) and boiling-water reactors (BWRs), (2) commercial high-level waste (CHLW) in the form of borosilicate glass in which commercial spent-fuel reprocessing wastes are incorporated, and (3) defense high-level waste (DHLW), also incorporated in borosilicate glass. The waste package is being designed for emplacement at a repository in the Topopah Spring Member of the Paintbrush Tuff at the Yucca Mountain site in Nevada. The reference horizon is located 350 m below the ground surface and 200 m above the

static water table. The composition of the gaseous phase and the vadose water makes the repository conditions slightly oxidizing.

Selecting the materials to be employed in the waste-package container is the responsibility of the Metal Barrier Selection and Testing Task Group of the Nevada Nuclear Waste Storage Investigations (NNWSI) Project. Six candidate materials are currently under consideration. These materials include three iron- to nickel-based austenitic materials and three copper-based alloys. The austenitic materials are Types 304L and 316L stainless steels and Alloy 825. The copper-based alloys are CDA 102 (oxygen-free copper), CDA 613 (Cu-7Al), and CDA 715 (Cu-30Ni). Some of the criteria for the selection of the final metal-barrier material will relate to the stability of these materials in the repository environment.

The design criteria for the metal barrier require that the waste container maintain mechanical integrity for a period of about 50 yr after emplacement to permit retrieval of the nuclear waste during the preclosure phase of repository operation. The waste packages are required to provide substantially complete containment of the waste for a period of 300 to 1000 yr. The metal barrier is part of the engineered barrier system. During the containment period, the metal barrier will be exposed to a varying environment. A few years after emplacement, the surfaces of many of the containers will reach a maximum temperature of about 250°C. This temperature will decay to about 150°C within about 100 yr following emplacement. Other containers will reach lower temperatures because of lower heat output. This early time period will also include the highest gamma radiation field from the decay of the high-level waste. This radiation will promote radiolytic decomposition of the moist air near the container surfaces. The hydrogen evolved by this radiolysis process has the potential to significantly alter the metallurgical behavior of the container material.

This volume is one of eight that make up the survey of degradation modes [1]. The purpose of the survey is to characterize the candidate materials. The other volumes in the survey address oxidation and corrosion, stress corrosion cracking, localized corrosion, phase stability, and effects of welding on container integrity.

This volume addresses the possible effects of hydrogen on the candidate materials. It summarizes our review of the literature, highlighting areas in which significant data and results exist and also identifying areas in which very little data was found. The candidate materials are ranked with respect to degradation in a hydrogen environment.

A discussion of the methodology and extent of the literature search can be found in the Overview.*

2. Copper-Based Candidate Alloys

The copper-based candidate alloys that have been selected for consideration by the NWMP are CDA 102, CDA 613, and CDA 715. A representative composition of these materials is given in Table 1 [2]. The alloy CDA 102 is oxygen-free copper, and both CDA 613 and CDA 715 are essentially two-component alloys. The mechanical properties of the latter alloys are generally enhanced in comparison with those of the pure copper material. For purposes of comparison, Table 2 lists certain mechanical properties [0.2% yield stress (YS), elongation, and ultimate tensile strength (UTS)] at room temperature [3]. A review of the basic metallurgy of CDA 613 and CDA 715 is presented here to highlight the advantages and disadvantages of each material.

2.1 Basic Metallurgy of the Copper-Based Candidate Alloys

CDA 102 is essentially pure copper and will exhibit few, if any, metallurgical changes in mechanical properties under repository conditions. The mechanical strength of CDA 102 is primarily dependent upon the thermomechanical history of the specific part. The higher the degree of cold work, the greater the yield stress and creep

* J. C. Farmer, R. D. McCright, J. N. Kass, *Survey of Degradation Modes of Candidate Materials for High-Level Radioactive-Waste Disposal Containers, Overview*, Lawrence Livermore National Laboratory, Livermore, California, UCID-21362 Overview (1988).

Table 1. Compositions of the copper-based candidate alloys (wt%).

Alloy	Cu	Ni	Al	Mn	Sn	Fe	Zn	Other
CDA 102	99.95	—	—	—	—	—	<0.001	Pb < 0.001
								Cd < 0.001
								S < 0.0018
								Hg < 0.0001
								P < 0.003
CDA 613	90.82	0.005	6.75	0.16	0.20	2.46	0.01	Pb < 0.01
								Co < 0.01
CDA 715	69.18	29.60	—	0.51	—	0.53	0.07	Pb, 0.01
								P, 0.002
								C, 0.04
								S, 0.01

resistance. The impurity element that affects this material the most is oxygen in the form of Cu_2O precipitates. These precipitates are not wetted by molten copper and hence are found predominantly on the grain boundaries of the as-cast material. These oxide precipitates will be examined in greater detail in Sec. 3.

Figure 1 shows the copper-aluminum equilibrium phase diagram [4]. This binary system exhibits a number of interesting phase transformations between about 10 and 30 wt% aluminum. Note that a eutectoid decomposition occurs at 565°C and approximately 12 wt% aluminum. This is a martensitic transformation at slow cooling rates, where the β phase transforms to α_1 and γ_2 phases. This transformation may prove important when considering the conditions that will occur in the heat-affected zone (HAZ) of a closure seal. Figure 2 [5] shows a partial phase diagram for the copper-aluminum system in the region around 9 to 16 wt% aluminum in copper. This figure extends the lower temperature of the phase diagram to 0°C and highlights the complex phase transformations that take place in these materials. The effects of phase stability and transformation on the mechanical properties of the copper-aluminum system are dealt with in detail elsewhere [1].

Table 2. Mechanical properties of the copper alloys at room temperature [3].

Alloy	UTS[a] (10^3 psi)	0.2% YS[a] (10^3 psi)	Percent elongation
CDA 102	32–66	10–53	55–4
CDA 613	70–85	30–58	42–35
CDA 715	54–75	20–70	45–15

[a]Softest to hardest commercial forms.

The copper-nickel equilibrium phase diagram exhibits solid-solution behavior throughout the entire composition range, as shown in Fig. 3 [6]. This means that no precipitate phases are present under equilibrium conditions. This feature may have advantages when considering the HAZ at the closure seal of the container.

The mechanical properties of the annealed copper-based candidate alloys are an important factor in determining the final design geometry and material requirements of the container. A comparison of the tensile strength as a function of temperature for the copper-based candidate materials is given in Fig. 4 [7]. Note that at high temperatures, CDA 715 has significantly higher tensile strength than CDA 613 or CDA 102. Above about 177°C, the tensile strength of CDA 715 surpasses that of CDA 613. Under repository conditions (25°C < T < 250°C), CDA 613 and CDA 715 have significantly higher tensile strengths than CDA 102. These mechanical properties are a baseline for comparison of the effects of hydrogen on the mechanical and microstructural behavior of these materials in a repository environment.

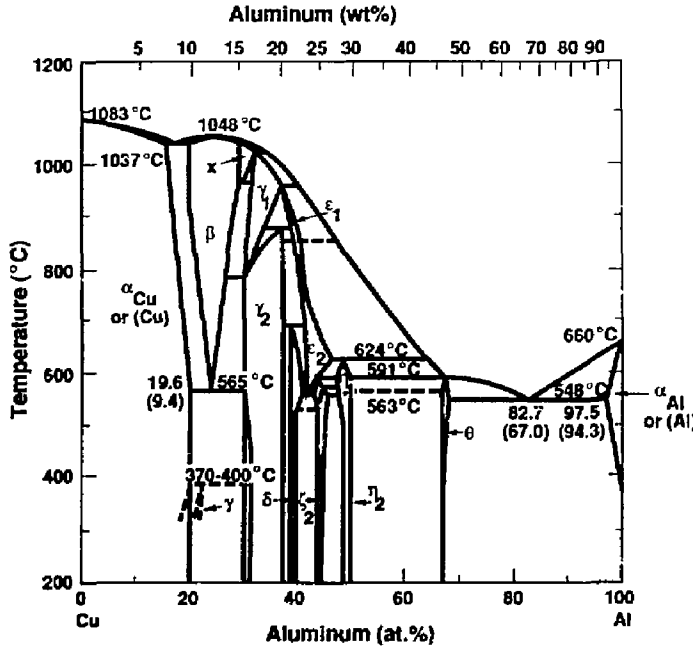

Figure 1. Copper-aluminum equilibrium phase diagram [4].

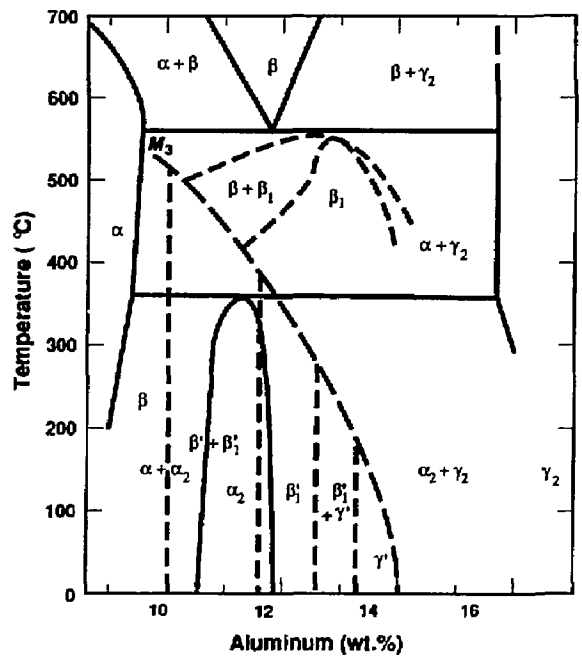

Figure 2. Copper-aluminum partial phase diagram [5].

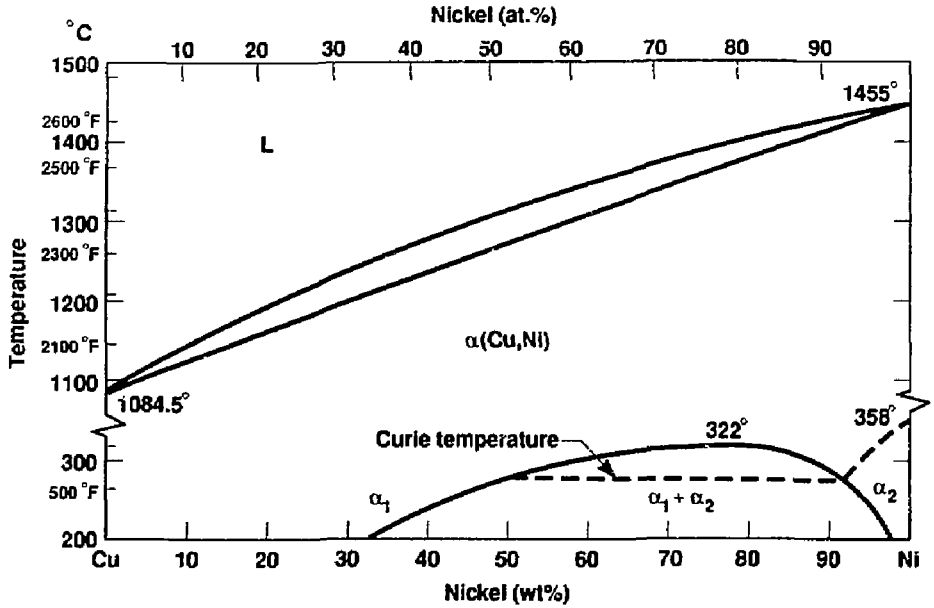

Figure 3. Copper-nickel equilibrium phase diagram [6]. The miscibility gap is proposed but has not been experimentally observed.

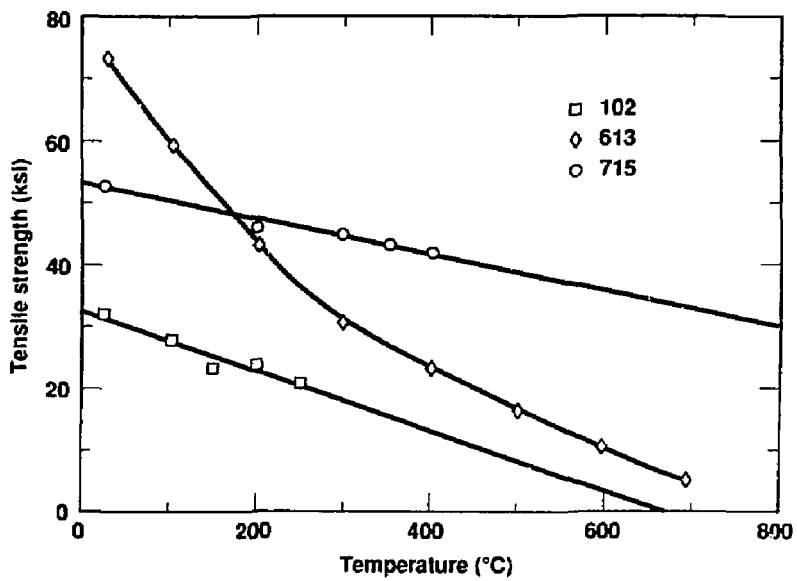

Figure 4. Tensile strength as a function of temperature for the copper-based candidate materials [7].

3. Effects of Hydrogen

Numerous articles in the technical literature review the effects of hydrogen on metals. McLellan and Harkins [8] completed an extensive review of the interaction of hydrogen with most metals, providing data from work completed through the mid 1970s. Previous reviews by Smith [9] and Mackay [10] summarize the extent of knowledge of the interaction of hydrogen with metals from the 1940s to the early 1960s, respectively. The degradation of the mechanical properties of copper and copper alloys exposed to a hydrogen environment has been extensively documented with respect to hydrogen and loss of ductility. A significant body of work addresses the mechanical properties of electrolessly deposited copper [e.g., 11, 12] and copper joined by various techniques [e.g., 13, 14]. These studies are of interest when considering joining techniques for the closure of the container.

A significant volume of work has been completed by the Europeans [15–20]. Beginning with the early investigations of Mattsson and Schuckher [15], the effects of hydrogen on mechanical properties and microstructure have been extensively documented.

3.1 "Hydrogen Sickness"

The mechanism of embrittlement of copper exposed to hydrogen was initially called Wasserstoffkrankheit or "hydrogen sickness" by the Germans. The degradation of high-purity copper exposed to a hydrogen environment is due to the formation of cavities on the grain boundaries. The mechanism, initially proposed by Ransley [21], was experimentally verified by Mattsson and Schuckher [15]. This mechanism describes the formation of cuprous oxide (Cu_2O) in the molten copper as the metal is cast. Since Cu_2O is not wetted by molten copper, the oxide is swept to the grain boundaries during the solidification process. The Cu_2O is not an extremely stable compound, with a Gibbs free energy of formation (ΔG_f) of –34.9 kcal/mole at 25°C. When the cast material is exposed to a hydrogen environment, the hydrogen dissociates on the surface of the metal, and diffuses along grain boundaries and throughout the matrix. This atomic hydrogen reduces the Cu_2O, forming water vapor (ΔG_f = –57.796 kcal/mole at 25°C) and metallic copper. Since the density of metallic copper is significantly greater than that of Cu_2O, a void space is readily formed at the site where the Cu_2O reduction occurred. This void is stabilized by the water vapor molecule and begins to grow as more Cu_2O reduction occurs along the same grain boundary.

This process leads to the "beaded microstructure" observed at the grain boundaries in nearly all cases in which hydrogen sickness has been documented. The formation of cavities on the grain boundaries quickly leads to a significant reduction in the ductility of the copper and ultimately to brittle intergranular fracture. The effects of hydrogen sickness have been noted in "pure" copper with an oxygen content as low as 22 atomic ppm [22]. The stoichiometry of the reaction indicates that twice as much hydrogen as oxygen is required. Under appropriate conditions, as little as 44 atomic ppm of hydrogen could therefore cause hydrogen sickness.

There are a number of methods used to prevent the degradation of copper by hydrogen sickness. The addition of small amounts of alloying elements such as zirconium, boron, phosphorus, or magnesium can tie up the oxygen in the form of stable oxides. These oxides cannot be reduced by hydrogen, so the formation of water vapor molecules is prevented within the copper matrix. Another advantage of these oxides is that they are wetted by molten copper. This wetting prevents the segregation of oxides to the grain boundaries during solidification of the melt. The resulting copper alloy contains impurity oxides dispersed throughout the metal matrix, which can provide strengthening of the alloy.

3.2 Degradation of Mechanical Properties

The formation of cavities filled with water vapor along the grain boundaries in copper has a significant effect on the mechanical properties. Kotova et al. [23] completed an extensive study of the degradation of mechanical properties of pure copper after it was annealed in a hydrogen atmosphere at temperatures between 600 and 960°C. Significant reduction in plasticity was noted for all specimens annealed in hydrogen and then tested to failure in a tensile testing device. The greatest loss of plasticity was noted for specimens tested to failure at temperatures between 200 and 500°C. Over this temperature range, the plastic

behavior of the copper decreased from 90% plasticity for copper containing no hydrogen to 40% plasticity for copper annealed in hydrogen at 850°C. Plasticity is defined by Kotova et al. to be the percentage reduction in cross-sectional area after fracture. Substantial loss of plasticity could lead to brittle failure, which might affect retrievability of the containers.

Kotova et al. also determined the hydrogen concentration as a function of anneal temperature for copper annealed in 1 atm of hydrogen and allowed to cool in the furnace under an atmosphere of hydrogen. Figure 5 shows the concentration of hydrogen as a function of anneal temperature. The plot has been expanded to illustrate the temperature range of interest to the NWMP.

The variation in mechanisms of penetration of hydrogen into copper from H_2 in the gas phase can be observed from the data provided by Kotova et al. Figure 6 shows the effect of annealing time on the uptake of hydrogen by copper at 850°C. Below an annealing time of 1 hr, the concentration of hydrogen that enters the copper is determined by one mechanism. Between 1 and about 25 hr, there is a transition region. Beyond about 25 hr, the concentration of hydrogen in copper is limited by another mechanism. These mechanisms were not addressed by Kotova et al. Potential rate-limiting steps include dissociation of hydrogen on the surface of the metal, grain boundary diffusion, and/or bulk diffusion. The three regimes that are illustrated in Fig. 6 suggest that great care must be taken when applying experimental data from the literature to potential repository conditions. At different experimental times and temperatures, the mechanism of hydrogen entry and migration through copper can vary significantly.

3.3 Solubility, Diffusivity, and Permeability

Copper is one of the many metals that dissolve hydrogen endothermically. The transport of hydrogen in copper also requires a significant driving force. The mechanism of hydrogen transport through copper, which was described previously, has been experimentally verified in a number of studies [15, 24–28]. Data from the literature have been reviewed and plotted throughout the temperature range of interest to the NWMP.

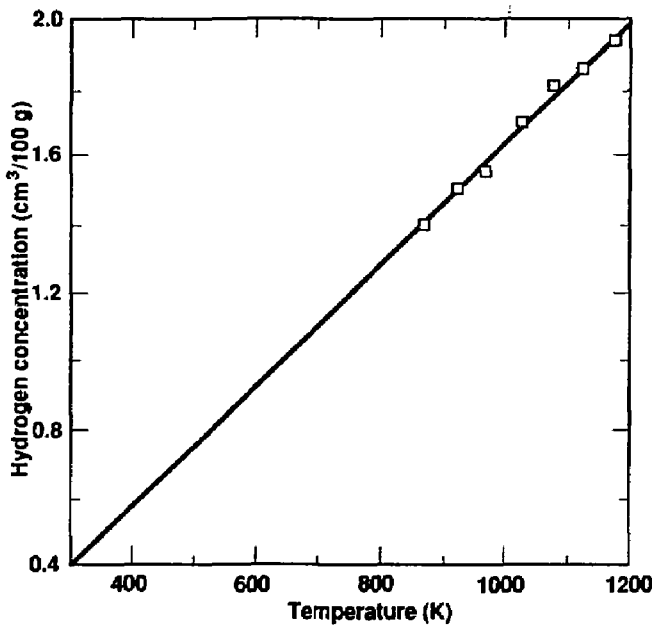

Figure 5. Retained hydrogen concentration vs temperature for high-purity copper [23].

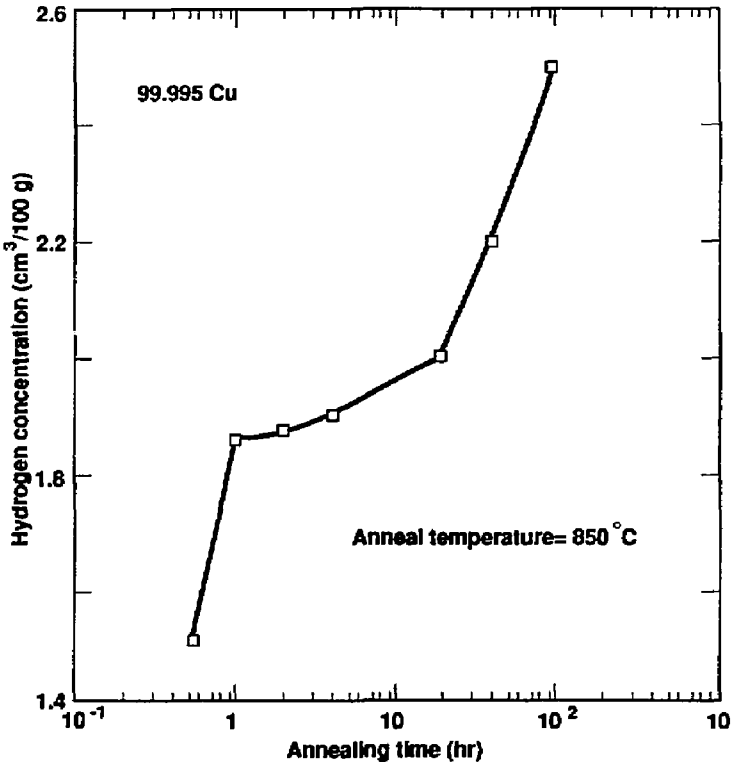

Figure 6. Retained hydrogen concentration vs anneal time in 1 atm H_2 for high-purity copper [23].

Figure 7 is a plot of the solubility of hydrogen in copper vs reciprocal temperature. The temperature range has been extrapolated down to 227°C to illustrate the extremely low solubility of hydrogen in copper under repository-relevant conditions. At 227°C, the solubility of hydrogen in copper is approximately 0.02 atomic ppm.

Another important physical parameter that will significantly affect the response of copper to hydrogen in a repository environment is the diffusivity of hydrogen in copper. Hydrogen's diffusion rate will determine its distribution in the bulk. Several studies [24–27] have been completed to determine the diffusivity of hydrogen in copper. Figure 8 shows a plot of diffusivity of hydrogen in copper vs reciprocal temperature for the temperature range 25 to 825°C. Recent work by Ishikawa and McLellan [25] determined the diffusivity of hydrogen in copper at room temperature. These data justify previous extrapolations of the diffusivity data to lower temperatures.

The ultimate measure of the transport of hydrogen through a copper component is the permeability. Begeal [28] completed an extensive study of the transport of hydrogen through copper and copper alloys. Figure 9 is a plot of the permeability of hydrogen through pure copper. Note that at the temperature of interest ($1/T$ = 0.003, T = 225°C), the permeability of hydrogen is extremely low ($K = 10^{-14}$ mole/s · m · $\sqrt{\text{Pa}}$). For 1 atm hydrogen at 225°C, the time required for hydrogen to reach its solubility limit at 1 mm is approximately 100 yr. Begeal also studied the effect of additions of alloy on the permeation of hydrogen through copper materials. He noted that the additions of alloying elements such as aluminum, beryllium, and silicon form an oxide layer on the surface, which further reduces the permeability of hydrogen.

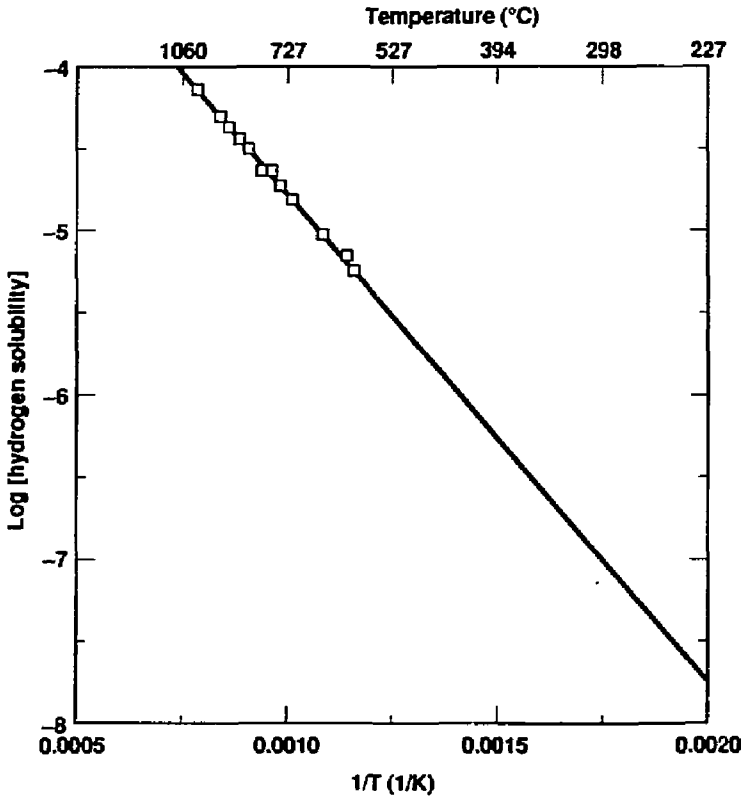

Figure 7. Hydrogen solubility (moles H per mole metal) as a function of temperature for copper [24].

It is interesting to note that the data presented in Figs. 7 through 9 are self-consistent. When variations in experimental conditions, including pressure of the hydrogen gas during the experiment, are considered, the product of the solubility data from McLellan (experiment completed at 1 atm hydrogen pressure) and the diffusivity data from Fig. 8 (experiments completed at 1 atm hydrogen pressure) yields a curve similar to the permeability data presented by Begeal in Fig. 9 (experiment completed at 0.1 atm hydrogen pressure).

3.4 Hydrogen Trapping in Copper

The precipitation and trapping of hydrogen in copper have been of significant interest to the fusion-reactor-materials community. The transport of hydrogen from a fusion plasma into the copper elements of containment magnets, with the ensuing degradation of mechanical properties, has inspired a number of studies of the precipitation and trapping of hydrogen in copper [20, 21, 29–30]. The endothermic nature of the dissolution of hydrogen in copper implies that small variations in temperature can produce significant supersaturation conditions. This phenomenon results in the precipitation of hydrogen in the form of bubbles in the metal matrix.

Wampler et al. [30, 31] developed models to explain the precipitation of hydrogen in a copper lattice. These models suggest that the increase in bubble volume during growth is due to plastic deformation of the copper lattice near the bubble. Wampler et al. also concluded that the precipitation of hydrogen in copper is a diffusion-limited process. Experiments completed by Wampler

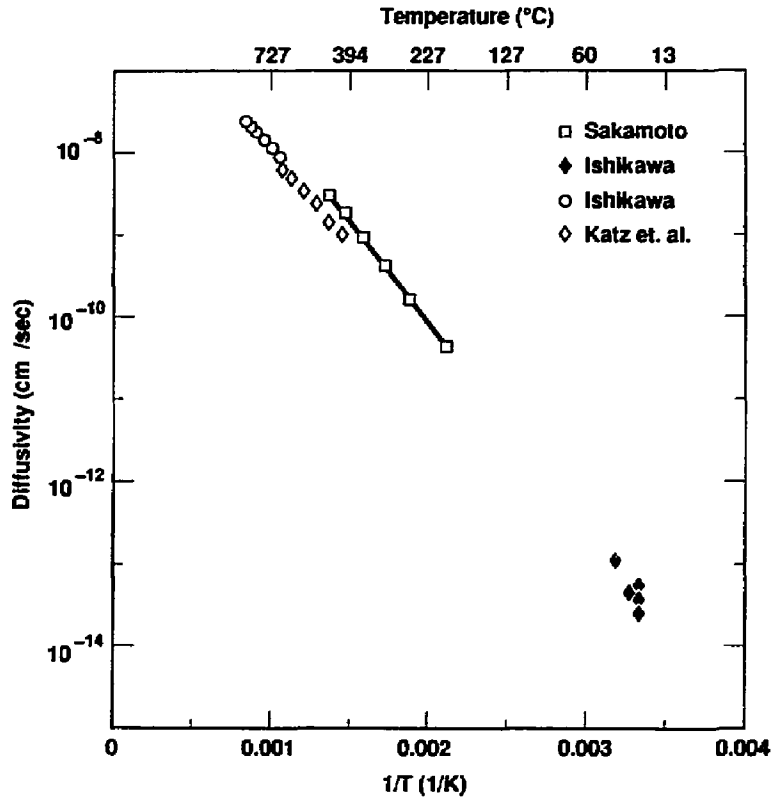

Figure 8. Hydrogen diffusivity in copper as a function of temperature [25–27].

et al. [30, 31] and Caskey and Pillinger [29] substantiate the model described above. Wampler measured changes in resistivity in hydrogen-saturated copper during isochronal anneals to determine the energy of solution of hydrogen. Wampler et al. noted that the hydrogen began to precipitate from the supersaturated solid solution at about room temperature. Untrapping of the hydrogen was substantially complete at about 50°C (323 K). Caskey and Pillinger measured the permeation of hydrogen through thin foils of copper and compared the relative permeation rates of annealed and cold-worked materials. Both studies noted an increase in hydrogen trapping with increasing concentrations of impurity and increasing level of cold work.

The direct application of these experimental results to repository-specific conditions is not recommended. To achieve the supersaturation conditions necessary to complete these experiments, the copper samples were subjected to extremely high hydrogen pressures (30–80 atm) and quenched from very high temperatures (1000°C) to very low temperatures (–150°C). The partial pressures of hydrogen and the temperature changes that will be present in the repository environment should be orders of magnitude less. Thus, determination of the hydrogen trapping and precipitation in the repository on the basis of these experimental data is impossible.

3.5 Effects of Hydrogen in Copper Alloys

A number of studies have been completed on the effects of hydrogen in copper-aluminum alloys similar to the candidate alloys under

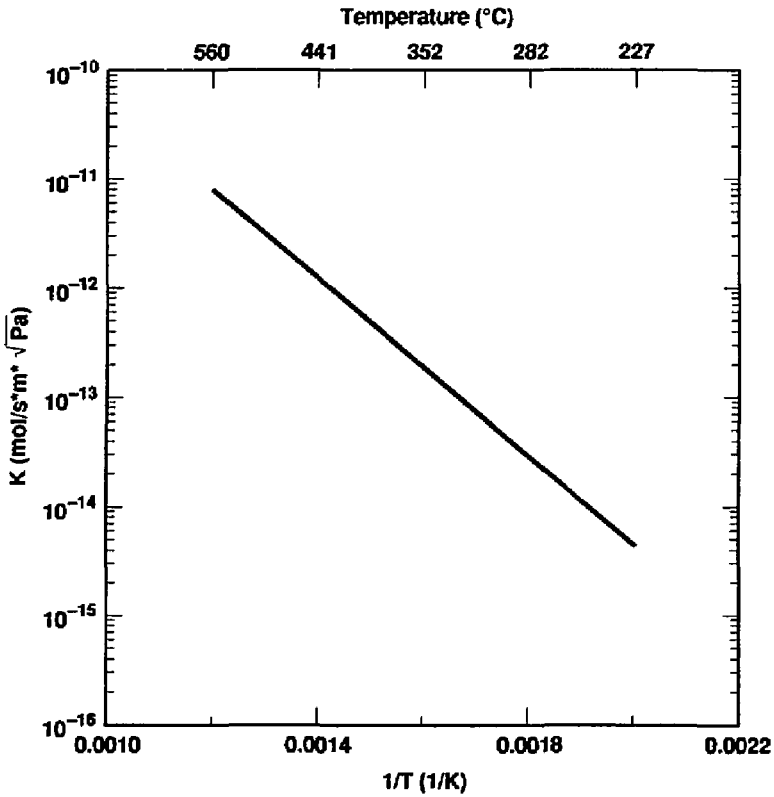

Figure 9. Hydrogen permeability in copper as a function of temperature [28].

consideration by the NWMP. Recent work by J. G. Byrne and others [32–35] employed transmission electron microscopy (TEM), scanning electron microscopy (SEM), mechanical testing, and positron annihilation to study the effect of hydrogen on copper and copper-aluminum alloys. In previous work, Himmler [36, 37] studied the solubility of hydrogen in copper alloys as a function of solute concentration.

Kim and Byrne [32] used the Doppler broadening of positron annihilation radiation to detect the trapping of hydrogen at dislocations within the metal matrix. They also used this technique to study the effect of additions of solute aluminum on the stacking fault energy of the alloy. Subsequent studies by Byrne and others [33–35] investigated the effects of cathodic charging, thermal charging, and variation in solute concentration on the microstructure and mechanical properties of copper-aluminum alloys. The results of these studies indicate that hydrogen charging of the copper and copper-aluminum alloys studied (Cu-4Al, Cu-8Al) reduced the fracture strain by about 5% in all cases. They also noted a concurrent increase in microhardness with hydrogen charging. The effect of the addition of aluminum solute atoms was to lower the stacking fault energy. Since the reduction in fracture strain was uniform for all alloys tested, the reduction in stacking fault energy in the copper-aluminum system appears to have no effect on the observed embrittlement characteristics. The trapping of hydrogen in the copper-aluminum alloys was noted to begin at a temperature of about 60°C, and detrapping occurred above about 110°C. This result is slightly different from the results noted by Wampler et al., in which detrapping was complete at about 50°C in pure copper. The embrittlement mechanisms in the copper-aluminum alloys were assumed to be similar to

the model of hydrogen trapping and precipitation proposed by Wampler et al. [30, 31].

There was very little information in the literature on the effects of hydrogen on the copper-nickel alloy system. The only work that was identified was that completed by Himmler [36, 37]. Himmler studied the effects of variation in solute concentration on the solubility of hydrogen. A summary of Himmler's results is shown in Fig. 10. This figure is a plot of the hydrogen concentration in a copper alloy as a function of concentration of solute atoms. Note that for additions of solute atoms of aluminum, tin, and gold, the solubility of hydrogen decreases with increasing solute concentration. The addition of silver solute atoms appears to have little effect on the solubility of hydrogen in copper. The addition of platinum solute atoms increases the solubility of hydrogen in copper slightly. The most dramatic increase in hydrogen solubility is noted for the addition of nickel solute atoms to the alloy. The addition of up to 25 wt% nickel appears to more than double the solubility of hydrogen in the alloy.

In light of the results presented by Himmler, the lack of data in the literature documenting the effects of hydrogen in copper-nickel alloys is not surprising. There is most likely little noticeable

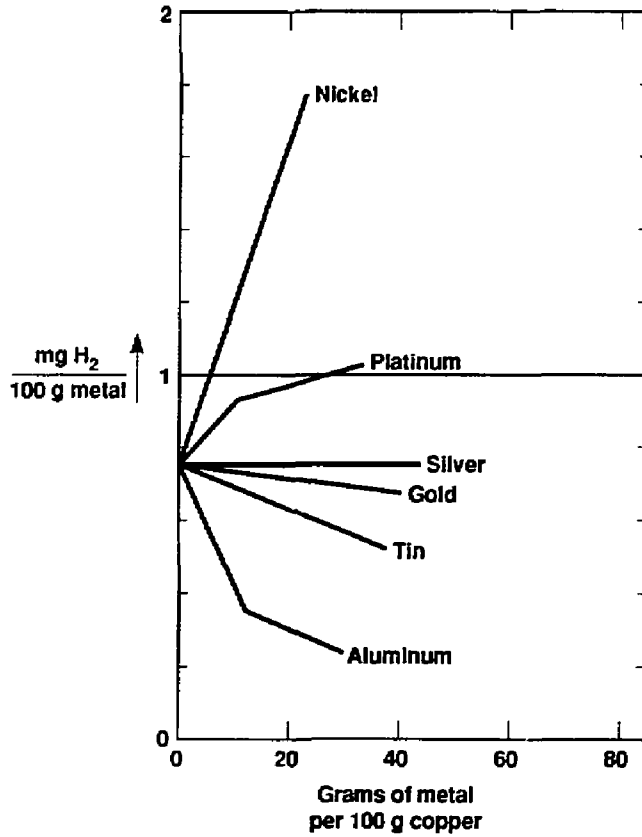

Figure 10. Hydrogen solubility in copper alloys as a function of alloying element content (wt%) at 1225°C. Note the increase in hydrogen solubility with increasing nickel content [36].

degradation in the mechanical or microstructural properties of copper-nickel alloys in a hydrogen environment. This would make the copper-nickel-hydrogen system uninteresting to study. However, an experimental effort to define the limits of hydrogen degradation of copper-nickel alloys is recommended to provide conclusive data verifying that the effects of hydrogen in the copper-nickel alloy would pose no problem for metal-barrier materials at repository conditions.

4. Summary of the Effects of Hydrogen in Copper-Based Alloys

A review of the literature has been completed on the effects of hydrogen on the candidate materials CDA 102, CDA 613, and CDA 715. There is a significant body of data documenting the effect called "hydrogen sickness," which is the reduction of Cu_2O impurities located on the grain boundaries. This reduction results in the formation of water molecules and a void space that is stabilized by the water vapor. The interconnection of these cavities results in significant degradation of the mechanical properties of the metal and subsequent brittle failure, which are observed experimentally. This phenomenon will occur with as little as 22 atomic ppm oxygen and, in the worst case, with just enough hydrogen to titrate the oxygen, that is, 44 atomic ppm.

In reviewing the literature, the solubility of hydrogen in copper was documented and the data were plotted over the temperature range of interest for repository applications. The diffusivity and permeability of hydrogen in copper were also documented over the same temperature range. Theoretical models and experimental evidence of the trapping of hydrogen in copper and copper-aluminum were noted. The detrapping temperatures varied slightly for pure copper (50°C) and the copper-aluminum alloy (110°C). The direct application of these models and data to repository conditions is not suggested because the hydrogen charging and trapping methods employed in these studies were very extreme.

There are very few available data on the effects of hydrogen in the copper-nickel alloy system. The results that are available indicate that the solubility of hydrogen increases with increasing nickel concentration. This result, coupled with the lack of data in the literature, suggests that there is probably little observable effect of hydrogen in the copper-nickel system.

5. Ranking of the Copper-Based Candidate Alloys

Considering the effects of hydrogen alone on the three copper-based alloys, the following ranking is proposed:

1. CDA 715
2. CDA 613
3. CDA 102

This ranking considers the solubility and documented response of each alloy system to a hydrogen environment. The most catastrophic material degradation was that of hydrogen sickness, that is, the formation of internal water from copper oxides. Since this has been noted in copper with as little as 22 atomic ppm oxygen content, it is apparent that some means of mitigating this effect is necessary for a repository material. The addition of deoxidizers is strongly recommended in CDA 102. The work of Byrne and others showed that both copper-aluminum and pure copper suffer degradation because of absorbed hydrogen. This degradation includes a 5% decrease in fracture strain. The increase in hydrogen solubility with increasing nickel content in the copper-nickel system may prove to be most advantageous. However, experimental verification of the response of CDA 715 to hydrogen under repository-relevant conditions is suggested prior to selection of this material for use in the NWMP containers.

6. Austenitic Candidate Alloys

The austenitic alloys being considered are Type 304L stainless steel, Type 316L stainless steel, and Alloy 825. They are candidate materials for the nuclear-waste isolation containers because of their relatively high strength and generally good corrosion properties. For purposes of comparison, Table 3 lists certain mechanical properties [0.2% yield stress (YS), elongation to fracture, and ultimate tensile strength (UTS)] for each of the alloys at room temperature [3, 38]. Table 4 lists the elemental composition ranges in wt% for each of the alloys [3, 38]. Also included in Table 4 are the compositions of Types 304 and 316 stainless steels. The "L" grade restricts the alloys to less than 0.03 wt% carbon. In addition, it also requires an increase in nickel content for the Type 304L stainless steel.

The low-carbon stainless steels have been chosen for their enhanced stress corrosion resistance over the alloys of higher carbon content. Sensitization of stainless steels of high carbon content occurs during thermal aging for $500°C < T < 800°C$ in time periods as short as 15 min [39–41]. Sensitization is the precipitation of metal carbides ($M_{23}C_6$), usually chromium carbides, on the grain boundaries, accompanied by a reduction in the concentration of the metal (chromium) in the region adjacent to the grain boundaries [42, 43]. Hydrogen and other corrosive species cause the sensitized alloys to stress-corrode more easily than the unsensitized alloys. Although they are more resistant, sensitization has been reported in Types 304L and 316L stainless steels, and Alloy 825 [39, 44–47].

In addition to enhancing resistance to sensitization, the lower carbon content in the steels reduces the possibility of the formation of methane (CH_4) within the steel [48]. Internal methane embrittles steels by forming high-pressure gas in grain boundaries. The internal stresses are sufficient to cause rupture. Also, under external loads, the internal methane can cause premature failure.

The resistance of the austenitic stainless steels to hydrogen-induced (-assisted) fracture has been correlated by Briant [49] with the relative stability of the austenite against martensite transformation. In fact, Briant [49] claims that embrittlement in the austenites is caused by martensite formation. An

Table 3. Mechanical properties of the alloys at room temperature [3, 38].

Alloy	UTS (10^3 psi)	0.2% YS (10^3 psi)	Percent elongation
304	95	35	65
316	85	37	65
825	100.5	43.7	43

Table 4. Elemental composition of the austenitic candidate alloys (wt%).

Element	Stainless steels				Alloy 825
	304	304L	316	316L	
C	0.08	0.03 max	0.08	0.03 max	0.05 max
Mn	2.00	2.00 max	2.00	2.00 max	1.0 max
Si	1.00	1.00 max	1.00	1.00 max	0.5 max
Cr	18.0–20.0	18.0–20.0	16.0–18.0	16.0–18.0	19.5–23.5
Ni	8.0–10.5	8.0–12.0	10.0–14.0	10.0–14.0	38.0–46.0
P	0.045	0.045 max	0.045	0.045 max	—
S	0.03	0.03 max	0.03	0.03 max	0.03 max
Cu	—	—	—	—	1.5–3.0
Ti	—	—	—	—	0.6–1.2
N	0.10	0.10	0.10	0.10	—
Mo	—	—	2.0–3.0	2.0–3.0	3.0
Fe	Bal.	Bal.	Bal.	Bal.	Bal.

austenite stability is bounded by a low strain-induced martensite transformation temperature, M_{d30}. Angel [50] has correlated M_{d30} with elemental composition in wt% for austenitic stainless steels:

$$M_{d30}(°C) = 413 - 462[C + N] - 9.2[Si] - 8.1[Mn] - 13.7[Cr] - 9.5[Ni] - 18.5[Mo]$$

The lower the value of M_{d30}, the more stable the alloy is against the martensite transformation. On the basis of this general correlation, the higher-alloyed Type 316 stainless steel should be more resistant than Type 304 stainless steel to hydrogen embrittlement.

7. Processes of Hydrogen Embrittlement

Although a number of mechanisms have been proposed to explain the embrittlement of austentic alloys by hydrogen, there appears to be no consensus with respect to any one mechanism. This section reviews experimental data available in the literature that addresses many of the proposed mechanisms. Numerous papers have been written on the subject of hydrogen embrittlement of Types 304 and 316 stainless steels. A large number of these papers have been catalogued with respect to the alloy, the type of experiment performed, and the experimental findings. This cataloguing is presented in the Appendix. Only representative findings about hydrogen embrittlement will be presented in this section. Unfortunately, only one published study on the effects of hydrogen in Alloy 825 was found. Fortunately, that study makes a direct comparison between Types 304 and 316 stainless steels [51].

Before discussing hydrogen embrittlement, it should be mentioned that most studies were performed using cathodic charging of the hydrogen. Because of the low solubility and diffusivity of hydrogen in the austenites, this form of charging results in high near-surface hydrogen concentration gradients. The bulk concentration of hydrogen is then uncharacterized for this type of experiment. These experiments are useful, though, to characterize trends. (Note: hydrogen solubility and diffusivity are discussed in the following section.)

The deleterious effects of hydrogen in the steels result primarily either from the hydrogen reacting with carbon to form internal methane or from bulk hydrogen itself degrading the mechanical properties of the metal. The methane formed builds up internal pressure and can cause fracture with or without external loads. The formation of internal methane in steels is usually restricted to those having high carbon contents (>0.1 wt%) [48] and has not been documented as a problem in the low-carbon austenitic materials.

High concentrations of hydrogen have been found to be deleterious in the austenitics. Extremely high concentrations of hydrogen can be formed in near-surface regions during high-fugacity cathodic charging of Types 304 and 316 stainless steels. These large hydrogen concentrations induce surface cracking in the pure austenitic materials [52, 53]. This surface cracking is primarily intergranular and results from hydrogen-induced strain fields. Stable martensite formation has often been reported to accompany surface cracking in Type 304L stainless steel [54, 55] and Type 316L stainless steel [56]. Surface cracking can be eliminated in Type 304L stainless steel if some of the austenite has been transformed to martensite by cold working [57]. Unfortunately, martensite itself degrades the mechanical properties of the metal, as explained below.

The degradation of mechanical properties of the austenitics has been shown to occur at relatively low bulk hydrogen atom concentrations. In general, though, tensile testing of Type 316L stainless steel [40, 44] and Type 304L stainless steel [39, 44, 58–60] in hydrogen for various charging conditions primarily shows degradation of ductility (elongation) with little change in the YS and UTS.

Graver [51] has studied the effect of low hydrogen concentrations on the elongation, UTS, and YS in all three austenitic alloys of interest. The hydrogen was cathodically charged for periods of 2 to 32 days. His findings are presented in Figs. 11 through 13. As can be seen from the figures, degradation of the YS and the UTS is small, while that of the elongation is much larger. The loss of elongation (ductility) means that the fracture is becoming more brittle. Elongation losses

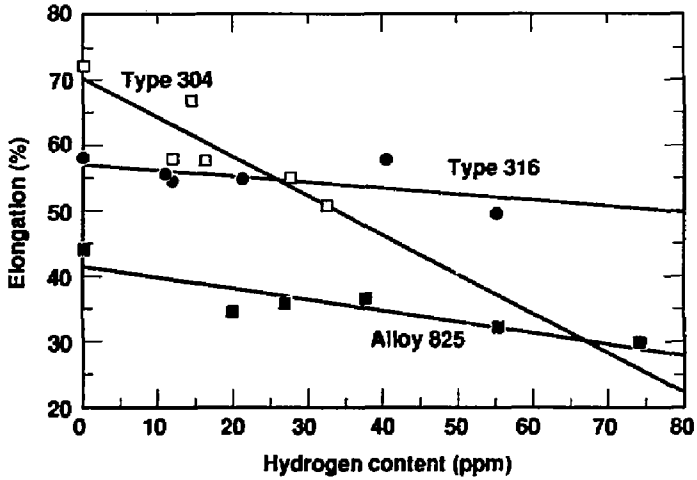

Figure 11. Eiongation vs hydrogen concentration for Types 304 and 316 stainless steels and high-nickel Alloy 825 [51].

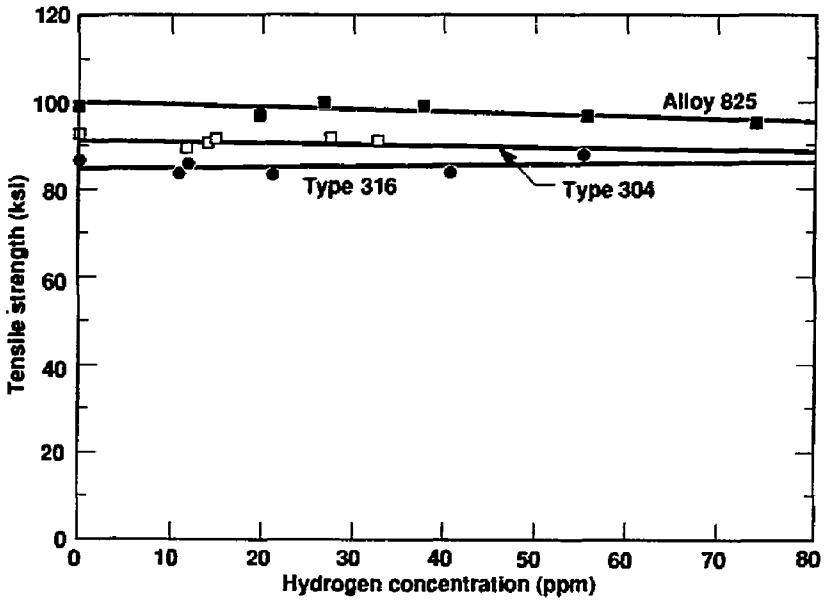

Figure 12. UTS vs hydrogen concentration for Types 304 and 316 stainless steels and high-nickel Alloy 825 [51].

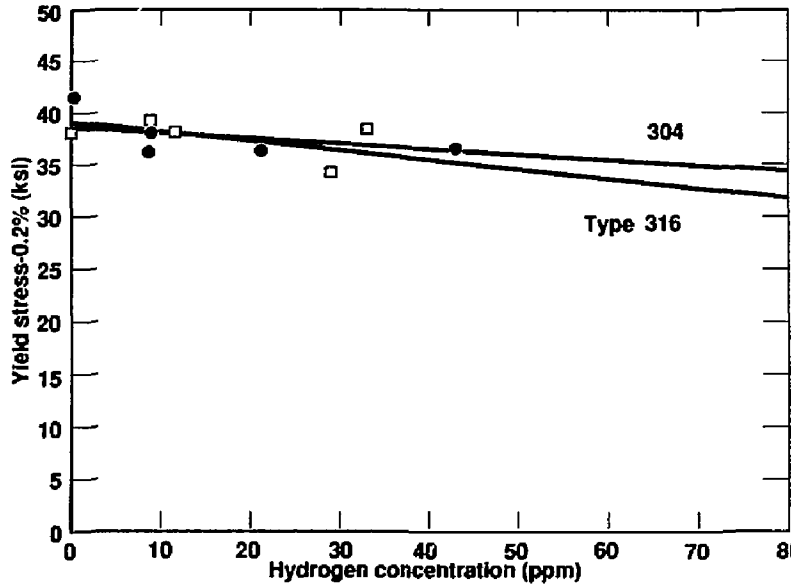

Figure 13. YS (0.2%) vs hydrogen concentration for Types 304 and 316 stainless steels [51].

at about 30 ppm hydrogen are greatest in Type 304 stainless steel (30% reduction) and somewhat less in Alloy 825 (16%) and Type 316 stainless steel (5%). The absolute magnitude of the percent elongation is less for Alloy 825 than for Type 304 or 316 stainless steel, but the tensile strength is greater for Alloy 825 than for Type 304 or 316 stainless steel. It should be noted that the loss in ductility occurs at hydrogen concentrations of the order of a few parts per million. In agreement with the above study by Graver, other combined studies of Types 304L and 316L stainless steels [40, 44] have shown that hydrogen charging of the steels primarily degrades the metal's ductility and that hydrogen embrittlement is much greater in Type 304 stainless steel than in Type 316 stainless steel.

Degradation in other mechanical properties has also been measured using high-fugacity cathodic hydrogen charging. Reductions in the UTS by 21 and 8%, respectively, for unsensitized Types 304L and 316L stainless steels have been measured by Minkovitz and Eliezer [44]. The accompanying reductions in elongation were 44 and 34% in Type 304L and Type 316L stainless steels, respectively. For Type 304L stainless steel, Holzworth [59] has also measured a reduction in UTS of about 30% after severe cathodic hydrogen charging.

Minkovitz and Eliezer [44] have also studied the effect of grain size and sensitization on the hydrogen embrittlement of Types 304L and 316L stainless steels. Sensitizing conditions were severe: 650°C for 24 hr. Their results are reproduced in Table 5. Under all test conditions, Type 304L stainless steel is more severely embrittled than Type 316L stainless steel. Coarser grain sizes and sensitization result in higher degradation of mechanical properties for both metals. In the worst case (coarse-grain and sensitized Type 304L stainless steel), this alloy showed a 77% reduction in elongation and a 44% reduction in UTS. In the best case, fine-grained Type 316L stainless steel, whether sensitized or annealed, showed a 34% reduction in elongation and less than an 8% reduction in UTS. Table 6 lists the mode of failure of the alloys under the test conditions. The fine-grained Type 316L stainless steel failed primarily by ductile fracture whether annealed or sensitized. At the other extreme, the coarse-grained

Table 5. Percent reduction in mechanical properties of Types 304L and 316L stainless steels [44]. Samples were tested while undergoing cathodic polarization. Properties are compared with those of uncharged samples. Note: ASTM 8 is a grain diameter of about 25 μm, and ASTM 6 is a grain diameter of about 50 μm.

Heat treatment and grain size	Percent reduction in properties		
	YS	UTS	Elongation
Type 304 L			
Annealed ASTM 8	7	16	37
Sensitized ASTM 8	6	20	54
Annealed ASTM 6	8	21	44
Sensitized ASTM 6	7	44	77
Type 316L			
Annealed ASTM 8	0	8	34
Sensitized ASTM 8	0	7	34
Annealed ASTM 6	0	5	38
Sensitized ASTM 6	0	12	42

Type 304L stainless steel failed by intergranular fracture when sensitized and by transgranular fracture when annealed.

The presence of α' martensite has been shown to have a varied effect on the mechanical properties of Type 304 stainless steel. Hanninen and Hakkarainen [61] studied the effect of 10 and 23% α' martensite on the mechanical properties of Type 304 stainless steel. Their results are reproduced in Table 7. The smaller amount of martensite appears to improve the mechanical properties over those of the solution-annealed material, while the larger amount definitely has a deleterious effect on the mechanical properties. It is interesting to note that brittle fracture occurred in all their samples, probably because of the very severe hydrogen cathodic charging conditions and the very high strain rate in the tensile test (see the Appendix).

Eliezer et al. [62, 63] have performed an extensive study of the slow crack growth (SCG) of a notched tensile sheet (1.6 mm thick) of Type 304 stainless steel for a variety of charging solutions. Their results are reproduced in Table 8. In an atmosphere of hydrogen gas, the appearance of SCG was dependent on the testing temperature. Hydrogen-induced SCG occurred in 16 psi H_2 at 80% of maximum load (55 ksi) at 25°C, but no SCG was recorded when the testing temperature was 160°C. Under more severe hydrogen charging conditions at room temperature, SCG occurred at lower loads than those used in hydrogen gas. It is interesting to note that the authors also studied the SCG in a more stable austenitic alloy, Type 310 stainless steel, and found no SCG under any of the hydrogen charging experiments.

As mentioned previously, most studies have used high-fugacity cathodic charging of hydrogen because of the low solubility of hydrogen in the austenites. With this technique, substantial concentrations of hydrogen can be obtained. Holzworth [59] has studied the recovery of the tensile properties of Type 304 stainless steel with aging in a nonhydrogen atmosphere. Figure 14 is

Table 6. Fracture modes of tensile-tested Types 304L and 316L stainless steels [44]. Samples were tested while undergoing cathodic polarization. Note: ASTM 8 is a grain diameter of about 25 μm, and ASTM 6 is a grain diameter of about 50 μm.

Heat treatment and grain size	Fracture mode (percent of surface)		
	Microvoid coalescence	Intergranular	Transgranular
Type 304L			
Annealed ASTM 8	15	—	85
Sensitized ASTM 8	30	70	—
Annealed ASTM 6	—	—	100
Sensitized ASTM 6	—	100	
Type 316L			
Annealed ASTM 8	85	15	—
Sensitized ASTM 8	85	15	—
Annealed ASTM 6	85	—	15
Sensitized ASTM 6	50	45	5

Table 7. Mechanical properties of Type 304 stainless steel tensile specimens tested at room temperature after hydrogen charging [61].

Condition	YS (ksi)	UTS (ksi)	Percent elongation to fracture
Uncharged	45.2	70.1	38
Solution-annealed	30.6	30.6	0
10% α′ martensite	44.7	44.7	0
23% α′ martensite	10.2	10.2	0

Table 8. Summary of results from the Type 304 stainless steel SCG study of Eliezer et al. [62]. Minimum time for crack growth is 3 hr.

Test conditions	Test temperature (°C)	Observations
16 psi H_2	25	SCG at > 80% maximum load (55 ksi) in air ; 4.5% α′ at brittle fracture surface
	160	No SCG; no α′
Air after charging 1 to 3 days in H_2SO_4 at 25°C	25	No SCG; 4.3% α′ at ductile fracture surface
Air after charging 2 to 3 days in $KHSO_4$ at 300°C	25	SCG at 75% max load (55 ksi); 11% α′ at brittle fracture surface
Stress while charging in H_2SO_4	25	SCG at 65% maximum load; 4% α′ at brittle fracture surface

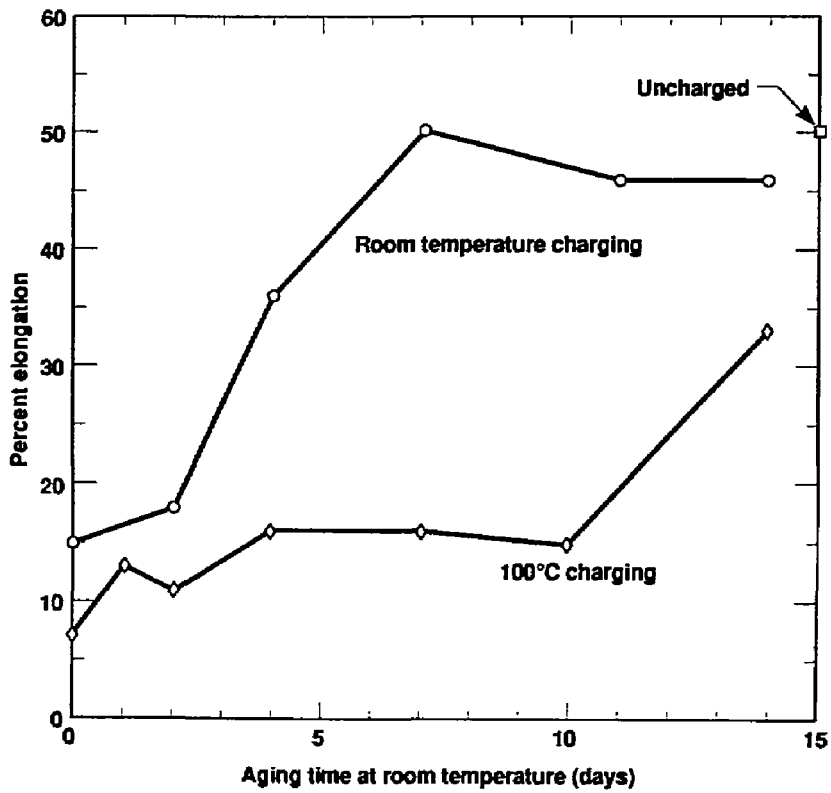

Figure 14. Recovery of elongation for Type 304L stainless steel with aging at room temperature after hydrogen charging at room temperature and 100°C. Charging conditions: 1N H_2SO_2 and 0.10 A/cm² [59].

a plot of his data for the elongation of the metal as a function of room-temperature aging for two charging temperatures. It is evident from the plot that the adverse effects of the hydrogen charging are reversible even at room temperature. Other studies have shown similar recovery of mechanical properties following aging in nonhydrogen atmospheres [64].

Since the containers in the repository will be at elevated temperatures for most of the recovery period, the effects of hydrogen on the alloys at elevated temperatures are of interest. Caskey [65] has performed such a study on bar samples of Type 304L stainless steel at temperatures up to 110°C. The samples were loaded with hydrogen at 200°C and 10 ksi for 1500 days. The results for the percent reduction in elongation vs test temperature are plotted in Fig. 15. There is no loss in ductility at 110 and –195°C. The largest degradations of elongation occur at 0 and –75°C. These results correlate well with those of Eliezer et al. [62, 63], where SCG in Type 304 stainless steel was found at 25°C but not at 160°C.

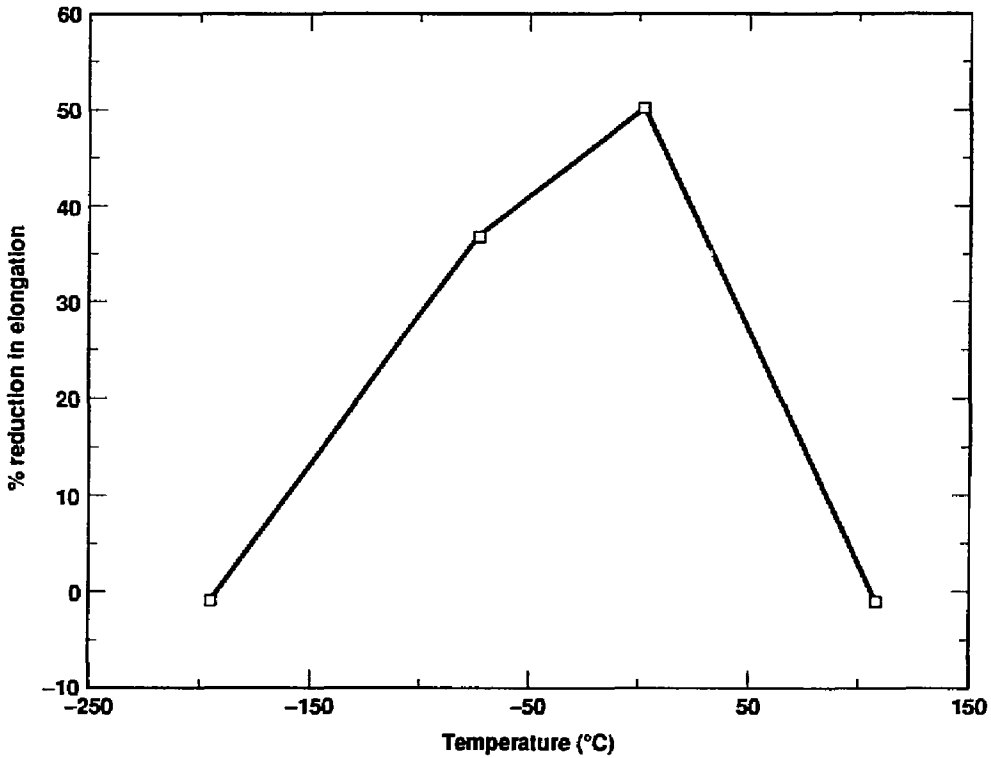

Figure 15. Percent reduction in elongation as a function of testing temperature for Type 304L stainless steel [65]. Note: at each temperature, the hydrogen bulk concentration is approximately 2×10^{-4} mol/cm^3.

8. Diffusivity and Solubility of Hydrogen

Experimental evidence indicates that hydrogen transport [58, 65, 66] and concentration [51] are critical in the embrittlement of the austenites. This section will examine the solubility and diffusivity of hydrogen in the candidate container materials. The values of these properties under storage conditions, 25 to 275°C, will be emphasized. Although there are no specific data for Type 316 stainless steel, it has been found in general that the properties of hydrogen vary little among the various austenitic stainless steels [67]. Therefore, the properties of hydrogen will be assumed to be the same in all the austenitic stainless steels. Unfortunately, there is no published literature on the properties of hydrogen for Alloy 825. The properties of hydrogen for nickel will be presented as a first approximation to those for the nickel-based Alloy 825.

The diffusivity of hydrogen in Type 304 stainless steel has been measured for 200°C < T < 350°C, and the best-fit equation is given by [67]:

$$D\ (\mathrm{cm^2/s}) = 7.69 \times 10^{-3} \exp[-12{,}700\ \mathrm{cal/mol})/RT]$$

This diffusivity has been extrapolated to the temperature range of interest to the Nuclear Waste Management Program (NWMP) and is plotted in Fig. 16. In the temperature range relevant to

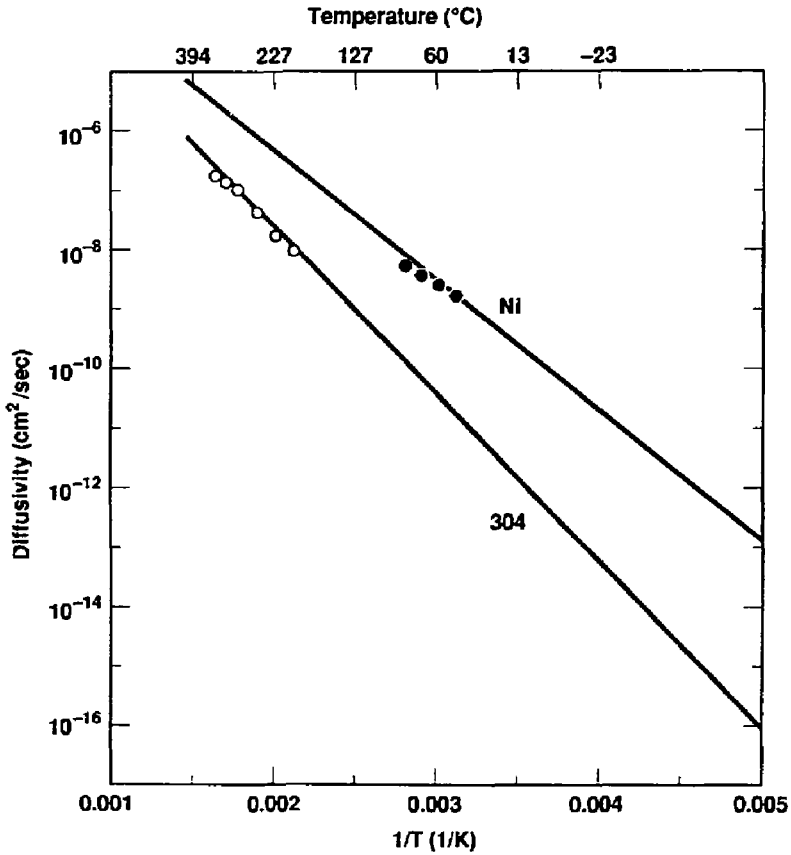

Figure 16. Hydrogen diffusivity for Type 304 stainless steel [67] and nickel [69], and the best-fit equations to the experimental data.

storage conditions, the hydrogen diffusivity is extremely small: 4×10^{-12} cm^2/s at 25°C and 7×10^{-8} cm^2/s at 275°C. These values are in agreement with other reported values [68].

To illustrate the slow hydrogen diffusion rate, the mean time (yr) required for hydrogen to diffuse 1 cm is plotted in Fig. 17. The diffusion time is calculated assuming random-walk conditions, that is,

$$t = x^2/4D$$

where t is time (s), x is distance (cm), and D is diffusivity (cm^2/s) [87]. At 25°C, the calculated time for 1 cm of diffusion is approximately 2000 yr, and at 225°C it is about 0.5 yr.

The best fit to hydrogen-diffusivity data in nickel (see Fig. 16) for numerous studies has been determined by Cermak and Kufudakis [69] and is given by:

$$D\ (\text{cm}^2/\text{s}) = 7.77 \times 10^{-3} \exp[(-9860\ \text{cal/mol})/RT]$$

These data should be considered as an upper limit to the diffusivity of hydrogen in Alloy 825, since alloying with iron should decrease its diffusivity. Nickel has a face-centered cubic structure, as does Alloy 825. Under conditions relevant to the

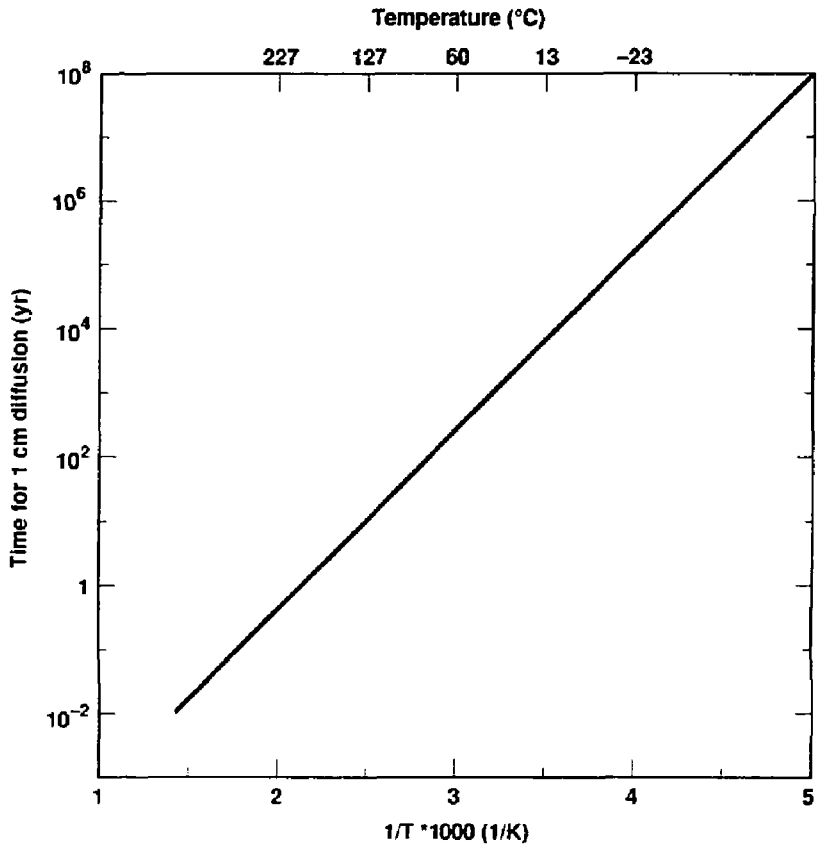

Figure 17. Time for hydrogen to diffuse 1 cm in Type 304 stainless steel as a function of temperature (see text).

repository, the diffusivity of hydrogen in nickel ranges from 5×10^{-10} cm^2/s (27°C) to 9×10^{-7} cm/s (277°C). These values are significantly higher than those for the austenitic stainless steels, but again, they are probably an upper limit to the actual diffusivity.

Absorption of hydrogen is endothermic in both the stainless steel austenites and nickel. Therefore, the solubility of hydrogen increases with increasing temperature. For solubility of hydrogen, just as for diffusivity, there is little variation among the stainless steel austenites [67]. Figure 18 is a plot of the best-fit equations of hydrogen solubility vs temperature for Type 304 stainless steel [67] and nickel [70]. For 200°C < T < 350°C, the variation of hydrogen solubility in Type 304 stainless steel with temperature and pressure is given by:

$$S \text{ (atomic ppm)} = 2.1 \exp[(-1100 \text{ cal/mol})/RT] \text{ (Pa)}^{-1/2}$$

where Pa is the pressure in pascals. For 350°C < T < 1400°C, the variation of hydrogen solubility in nickel with temperature and pressure is given by:

$$S \text{ (atomic ppm)} = (0.5 \log \text{Pa}) - 2.00 - 870/T$$

Enhanced transport of hydrogen by dislocations is thought to be critical for hydrogen

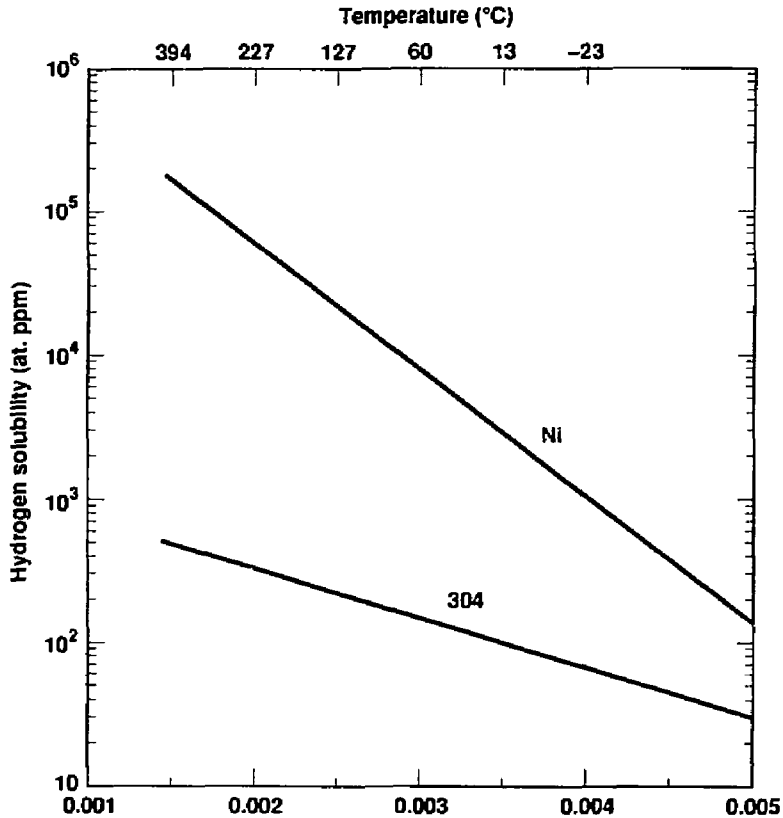

Figure 18. Plots of the best-fit equations to the experimental data for hydrogen solubility in Type 304 stainless steel [67] and nickel [70]. Note: experimental data are in the temperature range of 200 to 350°C.

embrittlement in the austenites [58, 66], though this is not the mechanism accepted by all [71]. The accelerated transport of hydrogen during plastic deformation has been documented for both nickel and Type 304L stainless steel [72]. If the dislocation transport of hydrogen is critical in embrittlement, then the concentration of hydrogen on dislocations is important. Caskey and Sisson [73] have calculated the concentration of hydrogen on dislocations, C_d, relative to that in lattice sites, C_l, for a severely cold-worked austenite (dislocation density 10^{12} cm/cm^3):

$$C_d = C_l 3.15 \times 10^{-4} \exp[(4400 \text{ cal/mol})/RT]$$

The ratio C_d/C_l is plotted vs $1/T$ in Fig. 19.

It is interesting that at temperatures greater than 0°C, most of the hydrogen resides in lattice sites rather than dislocation sites. In terms of the dislocation transport model, it is expected that embrittlement would be less severe at high temperatures because of the lower concentration of hydrogen dislocations. Caskey [65] has, in fact, observed this result (see Fig. 15). (The ductile fracture at –195°C can be explained by nonequilibrium distribution of hydrogen. That is, hydrogen is trapped in lattice sites after cool-down from the high-temperature charging. This occurs because of hydrogen's very low diffusivity at –195°C.)

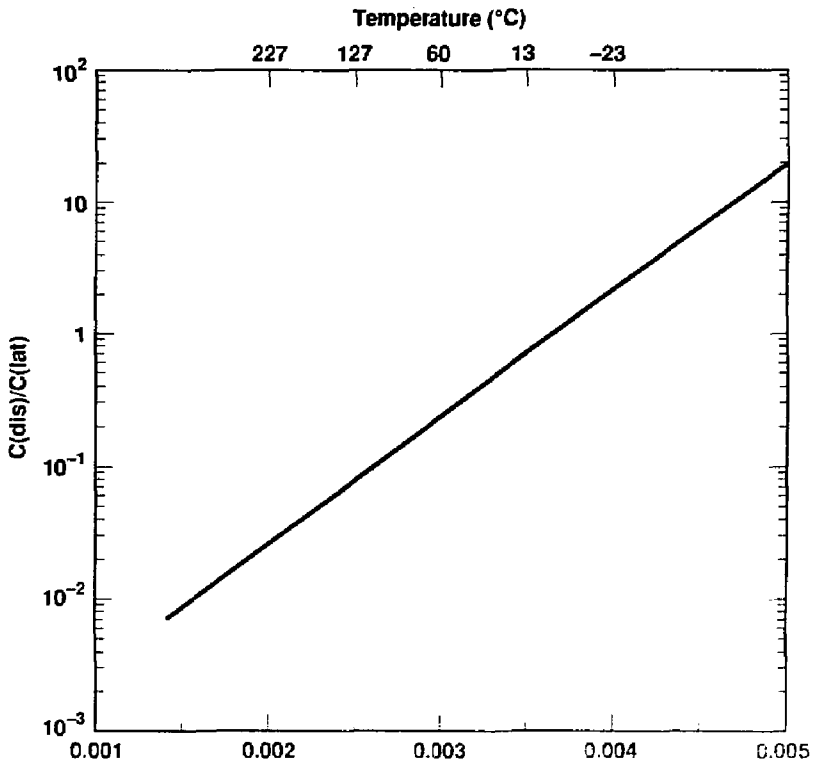

Figure 19. Ratio of hydrogen concentration on dislocations to that in the bulk lattice (see text).

9. Summary of the Effects of Hydrogen in Austenitic Candidate Alloys

A review of the literature has been completed on the effects of hydrogen on the austenitic candidate materials Types 304L and 316L stainless steels and Alloy 825. There is significant documentation to show that Type 316L stainless steel is less susceptible than Type 304L stainless steel to hydrogen embrittlement at room temperature. In general, both stainless steels are less susceptible to hydrogen when they have finer grain sizes and are not sensitized. However, the differences in the effects of hydrogen between sensitized and nonsensitized fine-grained Type 316L stainless steel are negligible.

There is a definite lack of literature on the effects of hydrogen in Alloy 825. The only published data indicate that Alloy 825 may be slightly more susceptible to hydrogen than Type 316 stainless steel. In the same study, it was shown that concentrations of hydrogen of the order of tens of parts per million were sufficient to cause degradation of the mechanical properties of all three alloys.

Some studies of hydrogen embrittlement in Type 304 stainless steel show that the alloy is less susceptible to degradation at elevated temperatures. In one study, no SCG in a hydrogen environment was reported at 160°C. In another study, no losses of ductility due to hydrogen were reported at 107°C. There were no reported studies at elevated temperatures for either Type 316 stainless steel or Alloy 825.

Solubilities and diffusivities of hydrogen in Type 304 stainless steel and nickel were documented. At room temperature, solubilities are of the order of parts per million and diffusivities are of the order of 10^{-10} to 10^{-12} cm^2/s in both materials. There are no data for Type 316 stainless steel, but the solubility and diffusivity of hydrogen are reported to be similar for different members of the austenitic stainless steel family. There are no data for hydrogen in Alloy 825, so data for pure nickel were presented as a first approximation.

10. Ranking of the Austenitic Candidate Alloys

Considering the effects of hydrogen alone on the three austenitic alloys, the following ranking is proposed:

1. Type 316L stainless steel, Alloy 825
2. Type 304L stainless steel

This ranking is based on phenomena of embrittling at room temperature, where many studies show that Type 304L stainless steel is more severely embrittled by hydrogen than is Type 316L stainless steel. The equivalent ranking of Type 316L stainless steel and Alloy 825 is based solely on Graver's work, where only small differences between the alloys were observed. There is a definite need for more experimental work on Alloy 825 to better characterize its susceptibility to hydrogen embrittlement.

If susceptibility to hydrogen embrittlement at higher temperatures is the critical criterion, then the ranking is not clear. There is definitely a lack of experimental results for all three alloys at elevated temperatures. But the experimental evidence that does exist for Type 304 stainless steel indicates that it is not as susceptible to embrittling at high temperatures as it is at room temperature. The degradation of the mechanical properties due to hydrogen at elevated temperatures may turn out to be indistinguishable among the three alloys.

11. Acknowledgments

This work was performed under the auspices of the U.S. Department of Energy by Lawrence Livermore National Laboratory under contract No. W-7405-ENG-48, and was supported by the Yucca Mountain Project.

12. References

1. D. B. Bullen, G. E. Gdowski, *Survey of Degradation Modes of Candidate Materials for High-Level Radioactive-Waste Disposal Containers, Vol. 1, Phase Stability*, Lawrence Livermore National Laboratory, Livermore, California, UCID-21362 Vol. 1 (1988). NN1.881220.0035

   G. E. Gdowski, D. B. Bullen, *Survey of Degradation Modes of Candidate Materials for High-Level Radioactive-Waste Disposal Containers, Vol. 2, Oxidation and Corrosion*, Lawrence Livermore National Laboratory, Livermore, California, UCID-21362 Vol. 2 (1988). NN1.881220.0036

   J. C. Farmer, R. A. Van Konynenburg, R. D. McCright, D. B. Bullen, *Survey of Degradation Modes of Candidate Materials for High-Level Radioactive-Waste Disposal Containers, Vol. 3, Localized Corrosion and Stress Corrosion Cracking of Austenitic Alloys*, Lawrence Livermore National Laboratory, Livermore, California, UCID-21362 Vol. 3 (1988). NN1.881220.0037

   J. C. Farmer, R. A. Van Konynenburg, R. D. McCright, G. E. Gdowski, *Survey of Degradation Modes of Candidate Materials for High-Level Radioactive-Waste Disposal Containers, Vol. 4, Stress Corrosion Cracking of Copper-Based Alloys*, Lawrence Livermore National Laboratory, Livermore, California, UCID-21362 Vol. 4 (1988). NN1.881220.0038

   J. C. Farmer, R. D. McCright, R. A. Van Konynenburg, G. E. Gdowski, *Survey of Degradation Modes of Candidate Materials for High-Level Radioactive-Waste Disposal Containers, Vol. 5, Localized Corrosion of Copper-Based Alloys*, Lawrence Livermore National Laboratory, Livermore, California, UCID-21362 Vol. 5 (1988). NN1.881220.0039

   M. J. Strum, H. Weiss, J. C. Farmer, D. B. Bullen, *Survey of Degradation Modes of Candidate Materials for High-Level Radioactive-Waste Disposal Containers, Vol. 7, Weldability of Austenitic Alloys*, Lawrence Livermore National Laboratory, Livermore, California, UCID-21362 Vol. 7 (1988). NN1.881220.0041

   D. B. Bullen, G. E. Gdowski, H. Weiss, *Survey of Degradation Modes of Candidate Materials for High-Level Radioactive-Waste Disposal Containers, Vol. 8, Weldability of Copper-Based Alloys*, Lawrence Livermore National Laboratory, Livermore, California, UCID-21362 Vol. 8 (1988). NN1.881220.0042

2. R. D. McCright, *FY 1985 Status Report on Feasibility Assessment of Copper Base Waste Package Container Materials in a Tuff Repository*, Lawrence Livermore National Laboratory, Livermore, California, UCID-20509 (September 30, 1985).
3. *Metals Handbook, Volume 2, Properties and Selection: Nonferrous Alloys and Pure Metals*, 9th ed., American Society for Metals, Metals Park, Ohio, 1979, pp. 237–490. NNA.890921.0078
4. M. Hansen, K. Anderko, *Constitution of Binary Alloys*, 2nd ed., McGraw-Hill Book Company, New York, 1958, pp. 84–90. NNA.891009.0004
5. J. Kwarciak, Z. Bojarski, H. Morawiec, "Phase Transformation in Martensite of Cu-12.4% Al," *Journal of Materials Science*, Vol. 21, 1986, pp. 788–792. NNA.890921.0079
6. M. Hansen, K. Anderko, *Constitution of Binary Alloys*, 2nd ed., McGraw-Hill Book Company, New York, 1958, pp. 601–604. NNA.891009.0004
7. C. H. Thornton, S. Harper, J. E. Bowers, *A Critical Survey of Available High Temperature Mechanical Property Data for Copper and Copper Alloys*, International Copper Research Association, New York (December 1983). NNA.890921.0080
8. R. B. McLellan, C. G. Harkins, "Hydrogen Interactions with Metals," *Materials Science and Engineering*, Vol. 18, 1975, pp. 5–35. NNA.890921.0081
9. D. P. Smith, *Hydrogen in Metals*, University of Chicago Press, Chicago, Ill., 1948.
10. K. M. Mackay, *Hydrogen Compounds of the Metallic Elements*, E. and F. N. Spon, Ltd., London, 1966.
11. S. Nakahara, Y. Okinaka, "Microstructure and Ductility of Electroless Copper Deposits," *Acta Metallugica*, Vol. 31, No. 5, 1983, pp. 713–724. NNA.890921.0082

12. Y. Okinaka, S. Nakahara, "Hydrogen Embrittlement of Electroless Copper Deposits," *Journal of the Electrochemical Society*, Vol. 123, No. 4, April 1976, pp. 475–478. NNA.890921.0083
13. S. Harper, V. A. Callcut, D. W. Townsend, R. Eborall, "The Embrittlement of Tough-Pitch Copper Windings in Hydrogen-Cooled Electrical Generators," *Journal of the Institute of Metals*, Vol. 90, 1961–62, pp. 414–429. NNA.890921.0084
14. E. Belkin, P. K. Nagata, "Hydrogen Embrittlement of Tough Pitch Copper by Brazing," *Welding Journal*, Vol. 54, February 1975, pp. 54s–62s. NNA.890921.0085
15. E. Mattsson, F. Schuckher, "An Investigation of Hydrogen Embrittlement in Copper," *Journal of the Institute of Metals*, Vol. 87, 1958–59, pp. 241–247. NNA.890921.0086
16. E. Kauczor, "Die Wasserstoffkrankheit des Kupfers," *Metall*, Vol. 19, No. 11, November 1965, pp. 1185–1187. NNA.890921.0087
17. O. Von Franque, E. Lindau, "Beobachtungen zum Einfluss des Gefüges und der Glühtemperatur auf die Wasserstoffversprödung von Kupfer," *Metall*, Vol. 20, No. 11, November 1965, pp. 1140–1143. NNA.890921.0088
18. J. Peterseim, G. Thummes, H. H. Mende, "Reduction of the Residual Resistivity of Thin Copper-Wires by Internal Oxidation," *Zeitschrift für Metallkunde*, Vol. 70, 1979, pp. 266–270. NNA.890921.0089
19. E. Albert, R. Kirchheim, E. Fromm, "Diffusion und Löslichkeit von Sauerstoff in Kupfer," *Case in Metallen*, Deutsche Gesellschaft fur Metallkunde, Darmstadt, F.R.G. (1979), pp. 45–49. NNA.890921.0090
20. B. Hammer, D. Lenz, P. Reimers, T. Dudzus, B. F. Schmitt, "Die Löslichkeit des Sauerstoffs in Reinskupfer," *Metall*, Vol. 38, No. 1, January 1984, pp. 41–45. NNA.890921.0091
21. C. E. Ransley, "The Diffusion of Oxygen in Copper," *Journal of the Institute of Metals*, Vol. 65, 1939, pp. 147–172. NNA.890921.0092
22. W. G. Wolfer, Sandia National Laboratories, Livermore, California, private communication (January 1987).
23. I. S. Kotova, V. M. Rozenberg, F. N. Strel'tsov, Zh.I. Dzeneladze, "Influence of Hydrogen on the Plasticity of Copper," *Fiz. Metal. Metalloved.*, Vol. 38, No. 4, 1974, pp. 858–863. NNA.890821.0093
24. R. B. McLellan, "Solid Solutions of Hydrogen in Gold, Silver and Copper," *Journal of Physics and Chemistry of Solids*, Vol. 34, 1973, pp. 1137–1141. NNA.890921.0094
25. T. Ishikawa, R. B. McLellan, "The Diffusivity of Hydrogen in Copper at Low Temperatures," *Journal of Physics and Chemistry of Solids*, Vol. 46, No. 4, 1985, pp. 445–447. NNA.890921.0095
26. L. Katz, M. Guinan, R. J. Borg, "Diffusion of H_2, D_2, and T_2 in Single-Crystal Ni and Cu," *Physical Review B*, Vol. 4, No. 2, July 1971, pp. 330–341. NNA.890921.0096
27. Y. Sakamoto, K. Takao, "The Electrochemical Determination of Diffusivity and Solubility of Hydrogen in Copper," *Journal of the Japan Institute of Metals*, Vol. 46, No. 3, 1982, pp. 285–290. NNA.890921.0097
28. D. R. Begeal, "Hydrogen and Deuterium Permeation in Copper Alloys, Copper-Gold Brazing Alloys, Gold, and the In Situ Growth of Stable Oxide Permeation Barriers," *Journal of Vacuum Science and Technology*, Vol. 15, No. 3, May/June 1978, pp. 1146–1154. NNA.890921.0098
29. G. R. Caskey, W. L. Pillinger, "Effect of Trapping on Hydrogen Permeation in Copper," in *Hydrogen in Metals*, American Society for Metals, Metals Park, Ohio, 1973, pp. 683–688. NNA.890921.0099
30. W. R. Wampler, T. Schoeber, B. Lengeler, "Precipitation and Trapping of Hydrogen in Copper," in *Proceedings of the 2nd International Congress of Hydrogen in Metals, Paris, 1977*, 1B11. NNA.890921.0100
31. W. R. Wampler, T. Schoeber, B. Lengeler, "Precipitation and Trapping of Hydrogen in Copper," in *Philosophy Magazine*, Vol. 34, No. 1, 1976, pp. 129–141. NNA.890921.0101
32. J. J. Kim, J. G. Byrne, "Hydrogen/Dislocation Studies by Positrons in Cathodically Charged Cu and Cu-Al Samples," *Scripta Metallurgica*, Vol. 17, 1983, pp. 773–778. NNA.890921.0102
33. J. J. Kim, J. G. Byrne, "Mechanical and Kinetic Effects of Cathodic Hydrogen Charging of Copper and Cu-Al Alloys," *Materials Science and Engineering*, Vol. 74, 1985, pp. 201–214. NNA.890921.0103
34. Y. Pan, J. G. Byrne, "Thermal Charging Effects of Hydrogen in Copper and Cu-Al Alloys," *Materials Science and Engineering*, Vol. 74, 1985, pp. 215–223. NNA.890921.0104

35. J. J. Kim, J. G. Byrne, "Transmission Electron Microscopy and Scanning Electron Microscopy Studies of Hydrogen Effects in Copper and Cu-Al Alloys," *Materials Science and Engineering*, Vol. 76, 1985, pp. 181–185. NNA.890921.0105
36. W. Himmler, "Löslichkeit von Wasserstoff in Kupfer-Zink- und Kupfer-Nickel-Legierungen," *Zeitschrift für Physikalische Chemie*, Vol. 195, 1950, pp. 244–259. NNA.890921.0106
37. W. Himmler, "Die Kathodische Überspannung der Wasserstoffabscheidung an Legierungen," *Zeitschrift für Physikalische Chemie*, Vol. 196, 1951, pp. 205–211. NNA.890921.0107
38. *Source Book on Industrial Alloy and Engineering Data*, American Society for Metals, Metals Park, Ohio, 1978, pp. 185–207, 219–223. NNA.891018.0189
39. Y. Rosenthal, M. Mark-Markowitch, A. Stern, D. Eliezer, "Tensile Flow and Fracture Behaviour of Austenitic Stainless Steels after Thermal Aging in a Hydrogen Atmosphere," *Materials Science and Engineering*, Vol. 67, 1984, pp. 91–107. NNA.890921.0108
40. E. Minkovitz, D. Eliezer, "Hydrogen-Assisted Cracking of Sensitized 316L Stainless Steel," *Journal of Materials Science*, Vol. 16, 1981, pp. 2507–2511. NNA.890921.0109
41. C. L. Briant, "Hydrogen Assisted Cracking of Type 304 Stainless Steel," *Metallurgical Transactions*, Vol. 10A, February 1979, pp. 181–189. NNA.890921.0110
42. R. L. Cowan, C. S. Tedmon, "Intergranular Corrosion of Iron-Nickel-Chromium Alloys," in *Advances in Corrosion Science and Technology*, M. G. Fontana, R. W. Staehle, Eds., Vol. 3, 1973, pp. 293–401. NNA.890921.0111
43. S. Danyluk, I. Wolke, J. H. Hong, E. A. Loria, "Intergranular Fracture, Corrosion Susceptibility, and Impurity Segregation in Sensitized Type 304 Stainless Steel," *Journal of Materials for Energy Systems*, Vol. 7, No. 1, June 1985, pp. 6–15. NNA.890921.0112
44. E. Minkovitz, D. Eliezer, "Grain-Size and Heat-Treatment Effects in Hydrogen-Assisted Cracking of Austenitic Stainless Steel," *Journal of Materials Science*, Vol. 17, 1982, pp. 3165–3172. NNA.890921.0113
45. E. L. Raymond, "Mechanisms of Sensitization and Stabilization of Incoloy Nickel-Iron-Chromium Alloy 825," *Corrosion*, Vol. 24, No. 6, June 1968, pp. 180–188. NNA.891009.0034
46. O. W. Albritton, "A Study of Sensitization in Types 304 and 304L Stainless Steels Using Mossbauer Spectroscopy," *Corrosion*, Vol. 24, No. 12, December 1968, pp. 389–392. NNA.890921.0114
47. A. P. Majidi, M. A. Streicher, "Potentiodynamic Reactivation Method for Detecting Sensitization in AISI 304 and 304L Stainless Steels," *Corrosion*, Vol. 40, No. 8, August 1984, pp. 393–408. NNA.890921.0115
48. L. C. Weiner, "Kinetics and Mechanism of Hydrogen Attack of Steel," *Corrosion*, Vol. 17, No. 3, March 1961, pp. 137t–143t. NNA.890921.0116
49. C. L. Briant, "Hydrogen Assisted Cracking of Austenitic Stainless Steel," in *Hydrogen Effects of Metals*, I. M. Bernstein, A. W. Thompson, Eds., The Metallurgical Society of AIME, 1981, pp. 527–540. NNA.890921.0117
50. T. Angel, "Formation of Martensite in Austenitic Stainless Steels: Effects of Deformation, Temperature, and Composition," *Journal of the Iron and Steel Institute*, Vol. 177, May 1954, pp. 165–174. NNA.890921.0118
51. D. L. Graver, "Hydrogen Permeation and Embrittlement of Some Nickel Alloys," in *Corrosion of Nickel-Base Alloys*, American Society for Metals, Metals Park, Ohio, 1984, pp. 79–85. NNA.890921.0119
52. P. Rozenak, D. Eliezer, "Effects of Metallurgical Variables on Hydrogen Embrittlement in AISI Type 316, 321 and 347 Stainless Steels," *Materials Science and Engineering*, Vol. 61, 1983, pp. 31–41. NNA.890921.0120
53. H. Okada, Y. Hosoi, S. Abe, "Technical Note: Formation of Cracks in Austenitic Stainless Steels Cathodically Charged with Hydrogen," *Corrosion*, Vol. 26, No. 7, July 1970, pp. 183–186. NNA.890921.0121
54. M. L. Holzworth, M. R. Louthan, "Hydrogen-Induced Phase Transformations in Type 304L Stainless Steels," *Corrosion*, Vol. 24, No. 4, April 1968, pp. 110–124. NNA.890921.0122
55. E. Minkovitz, D. Eliezer, "TEM Study on the Formation of Microcracks in Connection with α'-Martensite," *Journal of Materials Science Letters*, Vol. 1, 1982, pp. 192–194. NNA.890921.0124

56. E. Minkovitz, M. Talianker, D. Eliezer, "TEM Investigation of Hydrogen Induced ε-hcp-Martensite in 316L Type Stainless Steel," *Journal of Materials Science*, Vol. 16, 1981, pp. 3506–3508. NNA.890921.0123
57. P. Lacombe, M. Aucouturier, J. Chene, "Hydrogen Trapping and Hydrogen Embrittlement; Some Recent Results on the Direct Observation of Hydrogen Trapping in Metals and Its Consequence on Embrittlement Mechanisms," *Hydrogen in Metals*, American Society for Metals, Metals Park, Ohio, 1973, pp. 79–102. NNA.890921.0125
58. M. R. Louthan, G. R. Caskey, J. A. Donovan, D. E. Rawl, "Hydrogen Embrittlement of Metals," *Materials Science and Engineering*, Vol. 10, 1972, pp. 357–368. NNA.890921.0126
59. M. L. Holzworth, "Hydrogen Embrittlement of Type 304L Stainless Steel," *Corrosion*, Vol. 25, No. 3, March 1969, pp. 107–115. NNA.890921.0127
60. A. W. Thompson, "Ductility Losses in Austenitic Stainless Steels Caused by Hydrogen," in *Hydrogen in Metals*, I. M. Bernstein, A. W. Thompson, Eds., American Society for Metals, Metals Park, Ohio, 1974, pp. 91–105. NNA.890921.0128
61. H. Hanninen, T. Hakkarainen, "On the Effects of α' Martensite in Hydrogen Embrittlement of a Cathodically Charged AISI Type 304 Austenitic Stainless Steel," *Corrosion*, Vol. 36, No. 1, January 1980, pp. 47–51. NNA.890921.0135
62. D. Eliezer, D. G. Chakrapani, C. J. Altstetter, E. N. Pugh, "The Influence of Austenite Stability on the Hydrogen Embrittlement and Stress-Corrosion Cracking of Stainless Steels," *Metallurgical Transactions*, Vol. 10A, July 1979, pp. 935–941. NNA.890921.0129
63. D. Eliezer, D. G. Chakrapani, C. J. Altstetter, E. N. Pugh, "Hydrogen-Induced Slow Crack Growth in Austenitic Stainless Steel," in *Proceedings of the 2nd International Congress on Hydrogen in Metals, Paris, 1977*, Vol. 1, 3F5. NNA.890921.0130
64. H. Hanninen, T. Hakkarainen, "Fractographic Characteristics of a Hydrogen-Charged AISI 316 Type Austenitic Stainless Steel," *Metallurgical Transactions*, Vol. 10A, August 1979, pp. 1196–1199. NNA.890921.0131
65. G. R. Caskey, "Fractography of Hydrogen-Embrittled Stainless Steel," *Scripta Metallurgica*, Vol. 11, No. 12, 1977, pp. 1077–1083. NNA.890921.0132
66. M. B. Whiteman, A. R. Troiano, "Hydrogen Embrittlement of Austenitic Stainless Steel," *Corrosion*, Vol. 21, No 2, February 1965, pp. 53–56. NNA.890921.0133
67. T. P. Perng, C. J. Altstetter, "Effects of Deformation on Hydrogen Permeation in Austenitic Stainless Steels," *Acta Metallurgica*, Vol. 34, No. 9, 1986, pp. 1771–1781. NNA.890921.0134
68. M. R. Louthan, R. G. Derrick, "Hydrogen Transport in Austenitic Stainless Steel," *Corrosion Science*, Vol. 15, 1975, pp. 565–577. NNA.890921.0136
69. J. Cermak, A. Kufudakis, "Diffusion-Elastic Phenomenon and Diffusivity of Hydrogen in Nickel," *Journal of the Less-Common Metals*, Vol. 49, 1976, pp. 309–322. NNA.890921.0137
70. *Gase und Kohlenstoff in Metallen*, E. Fromm, E. Gebhardt, Eds., Springer-Verlag, 1976.
71. A. J. West, M. R. Louthan, "Dislocation Transport and Hydrogen Embrittlement," *Metallurgical Transactions*, Vol. 10A, November 1979, pp. 1675–1682. NNA.890921.0138
72. J. A. Donovan, "Accelerated Evolution of Hydrogen from Metals during Plastic Deformation," *Metallurgical Transactions*, Vol. 7A, 1976, pp. 1677–1683. NNA.890921.0139
73. G. R. Caskey, R.D. Sisson, "Hydrogen Solubility in Austenitic Stainless Steels," *Scripta Metallurgica*, Vol. 15, 1981, pp. 1187–1190. NNA.890921.0140
74. Y. Rosenthal, M. Marc-Markowitch, A. Stern, D. Eliezer, "The Influence of Hydrogen on the Plastic Flow and Fracture Behavior of 316L Stainless Steel," *Scripta Metallurgica*, Vol. 15, 1981, pp. 861–866. NNA.890921.0141
75. D. Eliezer, A. Arbel, P. Roznak, "Hydrogen Induced Delay Failure of AISI 316L and 321 Types Stainless Steel," *Journal of Materials Science Letters*, Vol. 2, 1983, pp. 602–604. NNA.890921.0142
76. R. J. Walter, R. P. Jewett, W. T. Chandler, "On the Mechanism of Hydrogen-Embrittlement of Iron- and Nickel-Base Alloys," *Materials Science and Engineering*, Vol. 5, 1969–70, pp. 98–110. NNA.890921.0143
77. P. Maulik, J. Burke, "Hydrogen Induced Martensite Transformation in Austenitic Steels," *Scripta Metallurgica*, Vol. 9, No. 1, 1975, pp. 17–22. NNA.890921.0144

78. M. R. Louthan, J. A. Donovan, D. E. Rawl, "Effect of High Dislocation Density on Stress Corrosion Cracking and Hydrogen Embrittlement of Type 304L Stainless Steel," *Corrosion*, Vol. 29, No. 3, March 1973, pp. 108–111. NNA.890921.0145
79. A. W. Thompson, O. Buck, "Hydrogen Effects on Martensite Formation," *Metallurgical Transactions*, Vol. 7A, February 1976, pp. 329–331. NNA.890921.0146
80. C. L. Briant, "Hydrogen Assisted Cracking of Sensitized 304 Stainless Steel," *Metallurgical Transactions*, Vol. 9A, May 1978, pp. 731–733. NNA.890921.0147
81. S. P. Hannula, "The Effect of Pre-Existing Epsilon Martensite on the Hydrogen Induced Fracture of Austenitic Stainless Steel," *Scripta Metallurgica*, Vol. 17, No. 4, 1983, pp. 509–513. NNA.890921.0148
82. G. R. Caskey, "Effect of Hydrogen on Work Hardening of Type 304L Austenitic Stainless Steel," *Scripta Metallurgica*, Vol. 15, 1981, pp. 1183–1186. NNA.890921.0149
83. J. M. Rigsbee, R. B. Benson, "A TEM Investigation of Hydrogen-Induced Deformation Twinning and Associated Martensite Phases in 304-Type Stainless Steel," *Journal of Materials Science*, Vol. 12, 1977, pp. 406–409. NNA.890921.0150
84. R. Liu, N. Narita, C. Altstetter, H. Birnbaum, E. N. Pugh, "Studies of the Orientations of Fracture Surfaces Produced in Austenitic Stainless Steel by Stress-Corrosion Cracking and Hydrogen Embrittlement," *Metallurgical Transactions*, Vol. 11A, Sept. 1980, pp. 1563–1574. NNA.890921.0151
85. N. Narita, C. J. Altstetter, H. K. Birnbaum, "Hydrogen-Related Phase Transformations in Austenitic Stainless Steels," *Metallurgical Transactions*, Vol. 13A, August 1982, pp. 1355–1365. NNA.890921.0152
86. H. Andriamiharisoa, H. Habashi, J. Galland, P. Azou, "Cathodic Hydrogenation of Austenitic Alloys in Molten Salt Baths at 200° or 300°C; Study of Hydrogen Induced Embrittlement," *Advances in Fracture Research*, Pergamon Press, New York, 1981, Vol. 4, pp. 1889–1897. NNA.890921.0153
87. P. G. Shewmon, *Diffusion in Solids*, McGraw-Hill, New York, 1963.

13. Appendix: Catalog of Studies on the Effects of Hydrogen in Types 304 and 316 Stainless Steels

Table A1. Studies of the effects of hydrogen in Types 304 and 304L stainless steels.

Type	Sample preparation	Charging conditions	Hydrogen conc. (ppm)	Grain size	Test	Sample treatment	% reduction			Fracture mode	Ref.
							0.2% YS	UTS	Elong-ation		
304L		H2 gas phase 87 psi; 600°C	300-325		tensile 0.1 cm/min	annealed	2.6	3	37	brittle IG rumpled surface	39
304	1100°C 1 hr WQ	continuous cathodic 1N H2SO4 40 mA/cm2			tensile	1) annealed 2) sensitized 650°C 24 hr				mixed ductile & brittle mostly IG	41
304L		continuous cathodic 1N H2SO4; RT 50 mA/cm2		ASTM 8	tensile 0.005 cm/min	1) annealed 2) sensitized 650°C 24 hr	7 6	16 20	37 54	TG with some ductile IG with some ductile	44
304L		continuous cathodic 1N H2SO4; RT 50 mA/cm2		ASTM 6	tensile 0.005 cm/min	1) annealed 2) sensitized 650°C 24 hr	8 7	21 44	44 77	TG IG	44
304		cathodic RT 0.5 A/cm2			tensile			17		surface cracking	53
304L		cathodic 1N H2SO4 RT 0.5 A/cm2			monitor microstructure					surface forms martensite and expands austenite lattice	54
304L	1100°C 1hr WQ	cathodic 1N H2SO4; RT 0.1 A/cm2			monitor microstructure					surface forms martensite	55
304L		H2 gas phase 10 ksi; 100°C 30 days	5 cc/cc		tensile at RT		0	11	55		58

Table A1. (Continued)

Type	Sample preparation	Charging conditions	Hydrogen conc. (ppm)	Grain size	Test	Sample treatment	% reduction			Fracture mode	Ref.
							0.2% YS	UTS	Elong-ation		
304L		H2 gas phase 10 ksi; RT			tensile		-11	11	35		58
304L		cathodic 1N H2SO4 0.1 A/cm2; 24 hr			tensile 0.03 cm/min		-7	33	76		59
304L	720°C 16 hr	H2 gas phase 10 ksi; 200°C 2 months	70		tensile at RT	annealed	0		55		60
304	1100°C WQ varied alpha' martensite by cold working	cathodic 1N H2SO4; 80°C 50 mA/cm2; 4hr			tensile 5 cm/min	1) soln annealed 2) 10% alpha' martensite 3) 23% alpha' martensite	33 0 78	56 36 85	100 100 100	brittle quasi-cleavage	61
304	1100°C 2 hr WQ	continuous cathodic 1N H2SO4; RT 40 mA/cm2			SCG; 3 hr min time for growth	annealed				25°C: SCG for > 36ksi TG with ductile fracture after crack initiation	62
304	1100°C 2 hr WQ	H2 gas phase 16 psi			SCG; 3 hr min time for growth	annealed				25°C: SCG for > 43.5 ksi; TG fracture at 55 ksi 160°C: no SCG	62
304	1100°C 2hr WQ	cathodic KHSO4; 400°C 40 mA/cm2; 2-3 days			SCG; 3 hr min time for growth	annealed; tested at RT				25°C: SCG for > 41 ksi TG with ductile fracture after crack initiation	62
304L		H2 gas phase 10 ksi; 200°C 1449 days			tensile 0.05 cm/min	1) 107°C 2) 0°C 3) -75°C 4) -195°C	-8 -6 -8 -10	-7 25 19 4	-1 50 37 -1	ductile brittle brittle ductile	65

Table A1. (Continued)

Type	Sample preparation	Charging conditions	Hydrogen conc. (ppm)	Grain size	Test	Sample treatment	% reduction			Fracture mode	Ref.
							0.2% YS	UTS	Elong-ation		
304L		H2 gas phase 10 ksi; RT			tensile			13	9		76
304L	1100°C AC	cathodic 1N H2SO4; 303°C or 100°C			surface cracking with alpha' martensite formed						77
304L		continuous H2 gas phase 10 ksi; 155°C		76 microns	tensile		0	12	64	quasi-cleavage with surface cracking	78
304L	1000°C WQ	H2 gas phase 1 atm; 830°C; 2 hr	450	20 microns	monitor alpha' martensite during tensile tests					no enhancement of martensite during tensile test	79
304	1100°C WQ	H2 gas phase 25 psi; RT			slow strain rate 1.2 cm/min 0.05 cm/min	1) annealed 2) sensitized: 650°C 24 hrs				sensitized: IG for slow rate (40-60%) unsensitized: IG 1%	80
304	1060°C 20 min WQ	cathodic 1N H2SO4 50 mA/cm2; 2hr			monitor microstructure	cold working to form martensite				martensite increases surface cracking	81
304L		H2 gas phase 10 ksi; 350°C		ASTM 7 ASTM 6 ASTM1	tensile 0.051 cm/min		0			hydrogen has no effect on YS	82
304		cathodic RT 0.2 A/cm2			monitor microstructure					surface martensite formation	83

Table A1. (Continued)

Type	Sample preparation	Charging conditions	Hydrogen conc. (ppm)	Grain size	Test	Sample treatment	% reduction			Fracture mode	Ref.
							0.2% YS	UTS	Elong-ation		
304		cathodic			monitor microstructure					phase transformation of fracture surfaces	84
304		cathodic			monitor microstructure					phase transformation of fracture surfaces	85
304L	1050°C 1 hr WQ	cathodic molten salt baths			tensile RT 0.05 cm/min	1) 200°C charged 2) 300°C charged		39 23	56 35	brittle mixed brittle and ductile	86

WQ, water-quenched
RT, room temperature
TG, transgranular
IG, intergranular
SCG, slow crack growth
AC, air-cooled

Table A2. Studies of the effects of hydrogen in Types 316 and 316L stainless steels.

Type	Sample preparation	Charging conditions	Hydrogen conc. (ppm)	Grain size	Test	Sample treatment	% reduction			Fracture mode	Ref.
							0.2% YS	UTS	Elong-ation		
316L		H2 gas phase 87 psi; 600°C 170 hr	300-325	ASTM 11	tensile @ RT 0.1 cm/min	sensitized 600°C 170 hr	-7	-8	22	ductile with TG on sample edges; surface cracking 9.8% vol martensite	39
316L	1 hr 1100°C WQ	cathodic 1N H2SO4; RT 15 days			tensile 0.005 cm/min	1) annealed 2) sensitized 650°C 24 hr	0 0	0 0	8 21	1) MVC 2) IG with some MVC	40
316L	1 hr 1100°C WQ	continuous cathodic 1N H2SO4; RT 50 mA/cm2			tensile 0.005 cm/min	1) annealed 2) sensitized 650°C 24 hr	0 0	5 10	21 49	1) ductile 2) IG	40
316L		continuous cathodic 1N H2SO4; RT 50 mA/cm2		ASTM 8	tensile @ RT 0.005 cm/min	1) annealed 2) sensitized 650°C 24 hr	none none	8 7	34 34	1) MVC-85; IG-15 2) MVC-85; IG-15	44
316L		continuous cathodic 1N H2SO4; RT 50 mA/cm2		ASTM 6	tensile @ RT 0.005 cm/min	1) annealed 2) sensitized 650°C 24 hr	none none	5 12	38 42	1) MVC-85; TG-15 2) MVC-50; IG-45; TG-5	44
316		continuous cathodic 1N H2SO4; RT 50 mA/cm2		ASTM 9	tensile 0.005 cm/min	1) annealed 2) sensitized 650°C 24 hr	0 3	8 15	59 48		52
316		continuous cathodic 1N H2SO4; RT 50 mA/cm2		ASTM 7	tensile 0.005 cm/min	1) annealed 2) sensitized 650°C 24 hr	0 0	2 22	46 54	1) mix TG and MVC 2) mostly IG; some TG surface cracking	52
316		continuous cathodic 1N H2SO4; RT 50 mA/cm2		ASTM 11	tensile 0.005 cm/min	1) annealed 2) sensitized 650°C 24 hr	4 2	11 9	55 52	1) ductile with some TG 2) ductile with some TG	52
316	1 hr 1100°C WQ	cathodic 1N H2SO4; RT 100 mA/cm2; 1 hr			monitor epsilon martensite formation					epsilon martensite formed on surface	56

Table A2. (Continued)

Type	Sample preparation	Charging conditions	Hydrogen conc. (ppm)	Grain size	Test	Sample treatment	% reduction			Fracture mode	Ref.
							0.2% YS	UTS	Elong-ation		
316		H2 gas phase continuous 10 ksi	small		tensile	annealed	0	0	0		58
316	1hr 1100°C WQ	cathodic 1N H2SO4; 80°C 50 mA/cm2; 18hr			tensile 5 cm/min	1) RT 2) outgas 5 days 100°C			100 50	1) mostly TG some IG 2) ductile fracture w/ surface cracks no martensite formed	64
316L		H2 gas phase RT: 70 psi; 170 hrs 600°C; 70psi; 170 hrs			tensile @ RT 0.1 cm/min	1) annealed 2) sensitized 600°C 170 hr	3 3	3 5		1) mostly ductile 2) mostly ductile with some surface cracking	74
316L	2 hr 1100°C WQ	continuous cathodic 1N H2SO4; RT 50 mA/cm2			slow crack growth precracked constant load					edge: TG; center: ductile; no alpha' martensite	75
316		H2 gas phase 10,000 psi			tensile			0	-4.2		76

WQ, water-quenched
RT, room temperature
TG, transgranular
IG, intergranular
MVC, microvoid coalescence
YS, yield stress
UTS, ultimate tensile strength

The following number is for Office of Civilian Radioactive Waste Management Records Management purposes only and should not be used when ordering this document:

Accession Number: NNA.891222.0311